Electrification of the Hurricane

ROBERT A. BLACK

Hurricane Research Division, National Oceanic and Atmospheric Administration, Miami, Florida

JOHN HALLETT

Atmospheric Sciences Center, Desert Research Institute, Reno, Nevada

(Manuscript received 31 July 1997, in final form 4 August 1998)

ABSTRACT

A survey of reports of electrical activity in hurricanes and typhoons from flight notes and personal experience (18 years, >230 eyewall penetrations for R. A. Black; ~20 years for J. Hallett, plus that of others at the Hurricane Research Division), and perusal of flight notes dating from 1980, show that lightning in and within 100 km or so of the eyewall is usually sparse. However, occasionally, significant electrical activity (>one flash per minute) occurs in or near the eyewall. National Oceanic and Atmospheric Administration WP-3D aircraft penetrations through a number of storms relate the lightning occurrence to strong vertical velocity (>10 m s^{-1}) and the presence of supercooled liquid cloud droplets extending to temperatures below −20°C. Specific measurements of cloud properties during eyewall penetrations show that the supercooled cloud water content increases with upward velocities >~5.0 m s^{-1}, as does the presence of large (>2 mm) supercooled drops. Measurements at temperatures >−13°C show that the transition of supercooled cloud water to ice along an outward radial in all systems is associated with local electric fields (occasionally >20 kV m^{-1}) and negative charge above positive charge. In systems with stronger vertical velocity there is a larger region of supercooled cloud extending to lower temperatures where charge separation may occur, as judged by the presence of regions containing graupel, small ice, and cloud droplets. The ratio of ice to supercooled water increases radially outward from the eyewall and depends upon altitude (temperature). The spatial distribution of charge is further influenced by the relation of vertical velocity to the radial flow, with the upper charge regions tending to be advected outward. In symmetrical, mature hurricanes, supercooled water usually occurs only in regions at temperatures above about −5°C.

The upward transport of supercooled cloud water is limited by a balance between water condensed in the eyewall updraft and its erosion by ice in downdrafts descending in the outward regions of the eyewall. This ice originates from both primary and secondary ice nucleation in the updraft. This is consistent with an exponential increase in ice concentration, as the rate at which the ice particle concentrations increase depends on the production of secondary particles by preexisting graupel, some of which ultimately grow into new graupel, and its outward transport in the anvil flow aloft. Penetrations at temperatures as low as −15°C show the presence of electric fields consistent with specific laboratory-derived criteria for charge separated during ice–graupel collisions, given that a liquid water–dependent sign reversal temperature may occur. Such a reversal may result from either a changing temperature in the vertical, a changing cloud liquid water content in the horizontal, or a combination of the two.

Since cloud-to-ground (CG) lightning can be observed with remote detection networks that provide the polarity and frequency of CG lightning, there is potential that hurricane evolution may be detected remotely and that lightning may be usable as an indicator of a change in the storm intensity and/or track.

1. Introduction

Convective precipitation can be idealized in one extreme as coalescence rain formed entirely at temperatures above 0°C (as in Hawaii) and in a second extreme as convection at temperatures well below 0°C with all of the precipitation originating in the ice phase. In deep tropical convection, it is pertinent to inquire as to the amount of precipitation that originates as ice from high, cold levels and the amount that forms by coalescence in regions below and near the 0°C level. A parallel question, the central theme of this research, is concerned with the occurrence of electrification of such systems. Laboratory experiments suggest that the onset of significant electrification is associated with bouncing collisions between small ice and graupel growing from supercooled cloud droplets, followed by gravitational separation of charged particles. Key to assessing different microphysical processes is a knowledge of vertical velocities in these different situations. Vertical

Corresponding author address: Robert A. Black, Hurricane Research Division/AOML, 4301 Rickenbacker Cswy., Miami, FL 33149.
E-mail: rblack@aoml.noaa.gov

wind speeds <4–5 m s^{-1} will fail to carry raindrops >1-mm diameter aloft, and precipitation will fall out once formed, whereas vertical winds >8–10 m s^{-1} will carry all raindrops aloft, possibly reaching levels much colder than 0°C.

The ice phase evolves as cloud temperatures reach below 0°C to −20°C. The rate of transformation of supercooled water to ice depends on the details of the microphysical processes, particularly the existence of many supercooled raindrops and possible secondary ice formation. The organization of the motions, whether as individual convective clouds with varying shear or in a cyclonically rotating system, with inflow below and outflow aloft, determines in a critical way whether ice particles formed in earlier convection will provide ice embryos for newer convection.

Our work has a threefold purpose: first, to examine the vertical velocity and microphysical structure observed by aircraft penetration of several tropical cyclones; second, to relate this to the electrical state of the clouds as determined by visual lightning observations and aircraft measurements of electric fields; and third, to present our current state of knowledge on hurricane precipitation processes and suggest future research priorities for tropical rainfall studies.

2. Previous studies

Detailed electrical studies of hurricanes (here we use the term to cover tropical cyclones in the South Pacific Ocean and typhoons in the North Pacific Ocean) have been sparse. Anecdotal stories of aircraft penetrations of eyewalls ''lit up like Chinese lanterns'' exist, but the vast majority of nighttime penetrations of hurricanes with strong surface winds have had no visible lightning reported during the flight. Standard works on hurricanes (Simpson and Riehl 1981; Anthes 1982) scarcely mention the topic. Ludlum (1963) quotes an archaic account of a hurricane:

> Never did the sky look more terrible! For one whole day and night it blazed like a furnace, and the lightning broke forth with such violence that each time I wondered if it had carried off my spars and sails; the flashes came with such fury and frightfulness that we all thought the ships would be blasted.

More recently, lightning in hurricanes has occasionally been detected with land-based lightning detection networks (Black et al. 1986; Lyons and Keen 1994; Molinari et al. 1994; Samsury and Orville 1994). In all of the storms featured in these studies, the vast majority of the cloud-to-ground (CG) lightning strokes occurred in the outer rainbands, although as shown in Black et al. (1986), Lyons and Keen (1994), and Williams (1995), on occasion, lightning strokes delineate the eyewall. Lyons and Keen (1994) associated these events with the appearance of intense tropical ''supercell'' development in the eyewall. One such occurrence was concurrent with the strengthening of Tropical Storm Diana into a hurricane, and the other was observed just before the South Florida landfall of Hurricane Andrew. In the case of Hurricane Andrew, the storm was strengthening in the hours before landfall. We note, however, that few well-developed hurricanes have come within range of the National Lightning Detection Network (NLDN) since its deployment in the middle 1980s.

Of the storms featured in the literature, Hurricane Hugo (1989), a large, well-formed hurricane with maximum sustained winds of about 60 m s^{-1} (Samsury and Orville 1994), produced only 33 CG lightning strokes in the 18 h preceding and shortly after its landfall near Charleston, South Carolina. Hurricane Andrew (1992) was one of the strongest hurricanes to hit the United States in 50 years, yet it produced relatively little lightning (Molinari et al. 1994) compared to continental systems. In contrast, Hurricane Jerry (1989), a weak storm that barely reached hurricane strength, produced about as much lightning in an outer rainband as Andrew (Samsury and Orville 1994). These results show that the high horizontal wind speeds that characterize the hurricane are not a good predictor of electrical activity. We shall show that the distinction between electrically weak and active hurricanes is related to the presence of weak and strong updraft. If we can understand the physical and dynamical processes leading to the activity of individual convective storms, we can suggest the differences to be sought in electrically active or inactive hurricanes. We confine our studies to hurricanes over the ocean. Hurricanes dissipate rapidly on passage over land, as the source of energy of the storm (the transportation of heat and moisture from the warm sea surface) is greatly diminished.

We first examine characteristics of individual convective clouds over the tropical ocean (with sea surface temperatures above about 28°C), in that such convection produces cloud-base temperatures above about 20°C, with the potential for coalescence rain formation. Studies of summer cumulus clouds over Florida are included for comparison, as they are also relevant to understanding the electrical charge separation process and provide examples of clouds with relatively strong updrafts. The cloud condensation nuclei concentration of maritime air in which these clouds form is often low—less than 100 cm^{-3} at 0.5% supersaturation (Hudson and Frisbie 1991)—a result caused in part by nuclei removal by the precipitation process itself. It follows that some variability in precipitation from shallow, warm clouds may depend on local (island) nuclei sources, local induced convection, or interacting weak gust fronts produced by precipitation elsewhere. With high cloud-base temperature, coalescence precipitation is likely to occur at a level somewhat above or below 0°C, depending upon updraft vertical profiles (Lopez et al. 1985; Rutledge et al. 1992). Updraft velocities determined from aircraft penetrations in maritime convection during the Global Atmospheric Research Program Atlantic Tropical Ex-

periment (GATE) project (LeMone and Zipser 1980) are typically low (<5 m s^{-1}). Similar modest vertical velocities were found in hurricanes (Jorgensen et al. 1985), in the Pacific near Taiwan (Jorgensen and LeMone 1989), and in the northern Australia summer monsoon (Zipser and Lutz 1994).

However, in the absence of the ice phase, penetrations above the 0°C level in convection over land have much stronger vertical velocities, sometimes more than 25 m s^{-1}, which carry supercooled rain and cloud water to altitudes where the temperature is at least as cold as −15°C (Hallett et al. 1978; Willis et al. 1994). This latter study showed that the advent of both ice particles and a strong electric field is nearly simultaneous and extremely rapid. In addition to this, there is reason to expect an increasing vertical velocity with height, in part supported by aircraft observations with vertically pointing Doppler radar (Black et al. 1996).

The question of how the evolution of ice takes place is important to cloud electrification. Two conceptual approaches are commonly used: a Lagrangian approach, in which ice evolves in an ascending parcel (Willis and Hallett 1991); or a steady-state process in the interface between all supercooled water in the updrafts, with ice evolving in a region of weaker updraft (or downdraft) in a region of vertical shear (Willis et al. 1994). It is in this stage that charge separation and subsequent electrical activity might be expected to occur, as growing graupel particles and smaller ice particles interact.

Specifically, to separate charge on a microscopic scale, laboratory results (Takahashi 1978; Jayaratne et al. 1983; Saunders et al. 1991) show that it is necessary to produce small ice particles of 10s to 100s of μm in diameter, together with millimeter diameter low-density graupel particles that are growing in the presence of a supercooled cloud. In these laboratory experiments, the drop size distributions were not controlled and are probably different. From the above experiments, larger particles become positively charged for typical cloud liquid water contents ≤ 1 g m^{-3} at temperatures above −10°C. The drop size distribution changes graupel growth rate through the variation of the droplet collection efficiency with size (Brooks et al. 1997; Saunders and Peck 1998), as well as the fall velocity through size and changing density of accreted ice. In most of the experiments listed above, the rime was growing in the dry-surface mode. When graupel are in the wet growth regime, Saunders and Brooks (1992) show that little or no charge separation occurs. Thus the changing droplet size distribution, as well as temperature and liquid water content (LWC), need to be considered in the charge separation process (see Fig. 16 for a conceptual view).

In an environment with adjacent up- and downdrafts, a situation can be hypothesized where cloud properties change at a given level from all supercooled water in updraft, to all ice in downdraft, with varying concentrations of graupel, small ice, and cloud water between, interacting to produce different sign and magnitude of charge separation. In situ processes involving vapor growth on freshly rimed particles also produce positively charged particles at all temperatures; ice evaporation in downdrafts give negatively charged graupel (Dong and Hallett 1992). The former processes are more likely in the case of cloud growth with LWC and rapid ice growth by accretion and from vapor diffusion. On the macroscopic scale of the cloud, separation of charge results first from gravitational separation of particles carrying different signs of charge, followed by differential advection of net charge regions; both mechanisms are possible and necessary.

The criteria for an electrical discharge is related to the total separated charge available to feed the discharge. This process depends upon the separation of like-polarity charge on similarly sized particles following the changes in cloud water content and temperature. Secondary ice production during graupel growth (Hallett and Mossop 1974) is a probable source of ice particles at relatively high temperatures (−4° to −5°C), bearing in mind that it may occur at lower temperatures (−7° to −8°C) with increasing liquid water content (Foster and Hallett 1982; Heymsfield and Mossop 1984). Such processes also depend on the drop size distribution, particularly the presence of larger cloud droplets with a diameter >23 μm and smaller droplets with a diameter <12 μm (Mossop 1985). The drop size distribution at this level results from the initial cloud droplet formation at cloud base modified by entrainment and coalescence during its rise from below. Optimum charge separation processes are therefore likely to occur when the right proportion of graupel and ice particles is present in a supercooled cloud with these characteristics. This mix may occur in quite localized regions in the vertical shear zone between the LWC in the updraft and the ice in the downdraft.

Both the laboratory and theoretical results predict specific conditions for separation of charge. The uncertainty in these results concerns how much supercooled LWC is required at various temperatures to separate a given sign of charge, and it might be that both signs of charge are generated on larger particles in relatively close regions, depending on cloud liquid water content, droplet size distribution, and temperature. In this sense the hurricane provides a good place for such a study, as the demarcation between ice and supercooled water is well defined along a radial flight track through the eyewall or other strong convection. This idea focuses the analysis in the following case studies.

3. Conceptual framework

From the above considerations, a likely scenario is that ice particle collisions on actively growing graupel at moderate to high (>0.5 g m^{-3}) LWC and temperatures >-10°C and vapor growth on recently or weakly growing graupel are expected to produce positively charged large particles and a negative (inverted) dipole:

−
+,

with a negatively charged cloud top and a positively charged lower region. Ice particle collisions in low (<0.5 g m^{-3}) LWC at $T < -10$°C, and ice evaporation would be expected to give negatively charged large particles and negative lower cloud, with a positive cloud top and dipole:

+
−.

More important is that this sign of charge on larger particles also occurs at lower temperatures between −10° and −25°C and moderate LWC near 1 g m^{-3}. Note that in a deep (>~10 km, temperatures <−20°C, with LWC) system, this is consistent with a tripole structure with the upper positive charge associated with small particles, the middle negative region with small crystals moving up and graupel falling out, and the lower positive zone associated with graupel:

+
−
+.

Under somewhat stable conditions, advection of charged particles can result in layers of different polarity charge at different altitudes. Such layered-charge structures were observed in several midlatitude mesoscale convective systems (MCSs) near Oklahoma by Rust and Marshall (1996) and others. The variations of vertical profiles of charge distribution were shown in the pioneering studies of Simpson and Scrase (1937) discussed by Rust and Marshall (1996) and observed in aircraft measurements by Dye et al. (1986). These studies show that the dipole/tripole generalization is subject to wide variability, which is related to spatial redistribution of charged regions as a sloping dipole associated with the vertical shear of the horizontal wind in the convective regions.

The dynamical structure of the hurricane has been described by Jorgensen (1984a,b) and the microphysics by Black and Hallett (1986). These studies illustrate the existence of weak (<5 m s^{-1}) updrafts except in specific regions of the eyewall, where updrafts between 5 and 10 m s^{-1} are associated with LWC of 1–2 g m^{-3}. Ice particles occur primarily in association with strong downdrafts immediately outward of the eyewall cloud water containing updrafts. Occasionally, when the storm is undergoing a rapid intensification phase (Black et al. 1994), vertical wind speeds >20 m s^{-1} and many lightning discharges are observed. In such cases, the mixed-phase region extends to much higher altitudes than normal, large graupel >5 mm in diameter is observed in the updraft just above the melting level, and downdrafts are both dynamically and microphysically driven, initiated at levels far above the melting level (Black et al. 1994).

Our observations create a conceptual model (see Fig. 16) of ice initiation in the updraft at levels at or above 6 km (−5°C), downdraft initiation on the inside of the eyewall by mixing with dry air aloft, and electrical activity associated with a narrow mixed-phase region between the updrafts and downdrafts. Black and Hallett (1986) pointed out that the liquid water regions are often completely absent from a mature hurricane and that strong vertical velocities (as observed over land) are rare. The orbital motion of the ice around the eye (typically with a period of 0.5–1.5 h; Marks and Houze 1987) distributes ice around the eye rapidly and provides a natural seeding of all clouds from the eyewall outward for up to 100 km or more as it is carried in the anticyclonic cirrus-type outflow aloft over any convection below.

These considerations suggest that electrification resulting in lightning in a hurricane will be unlikely for storms with weak eyewall updrafts and sparse regions of supercooled cloud and graupel growth. Electrical activity will be more likely in eyewalls with substantial updraft, extensive regions of supercooled cloud in the temperature range −5 to −25°C, and regions of vertical shear. In such eyewalls, mixed-phase regions occur with graupel, supercooled cloud water, and vapor-grown ice crystals coexisting between all water (eyeward) and all ice (outward). Further, the existence of regions of supercooled cloud and rain aloft is most likely with weakly mixed strong updrafts and when any ice redistribution process is inefficient, as when the upper-level shear carries anvil ice away from a nearby developing cumulus. In the aircraft studies herein described, eyewall penetrations were examined in detail to determine the spatial distribution of the microphysical mix together with electric field deduced from airborne field mills for several hurricanes. Observations are interpreted considering the laboratory work and set into a wider context of tropical convection processes.

4. Aircraft instrumentation

Measurements were carried out on the National Oceanic and Atmospheric Administration WP-3D aircraft in association with the Hurricane Research Division, Atlantic Oceanographic and Meteorological Laboratory. Except for the airborne field mill system, all instruments are as given in Jorgensen (1984a). Analysis procedures for the 2D particle image data are as given in Black and Hallett (1986) and Black (1990). Briefly, these include removing defective images of all types, such as splashes, broken images, multiple subimages within an image, streaks, and images whose longest dimension is on the edge of the array. Images are sized by area according to their equivalent circle diameter. The time of occurrence of liquid drops and mixed-phase images were identified by visual inspection of the raw image data.

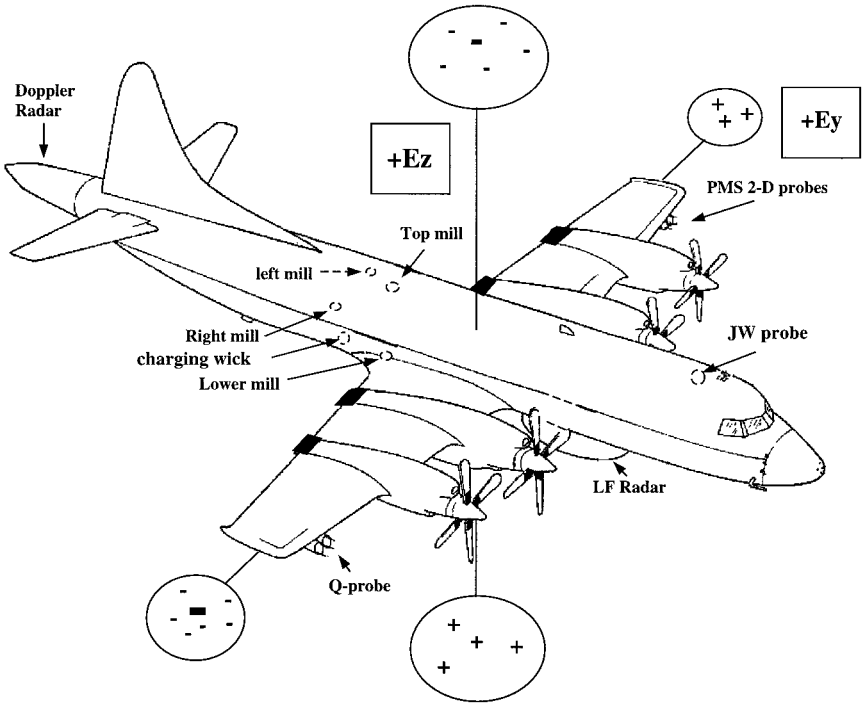

FIG. 1. Schematic of the field mill placement on the WP-3D.

Bulk ice particle density (required to compute ice water content) was calibrated using a two-step procedure to match the radar reflectivity computed from the size distributions with that at the aircraft position interpolated from the tail Doppler radar.

Cloud LWC is one of the more important variables to be measured. All of the devices available for this purpose in 1991–92 suffered from serious problems. The Johnson–Williams (JW) cloud liquid water meter is subject to destruction by graupel, drift of the zero LWC level (somewhat corrected in software), and occasional saturation by imperfect (corroded) connections. Overall, the JW (when available) has a minimum detectable signal of $\sim$0.1 g m^{-3} (Jorgensen 1984a). In ice cloud, the JW always responds as though 0.1–0.2 g m^{-3} of cloud LWC were present; this is also removed as a DC offset. In aggregated ice, particularly at temperatures >-5°C, the JW responds as though LWC were present, even though there is no updraft or evidence of LWC in the particle image data. These problems are noted in the case studies. The Particle Measuring Systems (PMS)–King liquid water meter suffers from problems similar to those of the JW, and it proved to be too fragile for use above the melting level in the hurricane. The PMS forward scattering spectrometer probe (FSSP) was useless for quantitative measurements because housekeeping data required to correct the concentrations for coincidence (multiple particles in the sample volume at once; Cooper 1988) and dead-time errors, which occur when particles enter the sample volume but are not sized because the probe is busy with the preceding particle (Cerni 1983; Baumgardner et al. 1985), were not recorded. Even if all possible corrections are made, Baumgardner (1983) suggested that the FSSP LWC accuracy was 54%–105% over the water content range of 0.02–5 g m^{-3}. Further, Gardiner and Hallett (1985) show that the FSSP cloud drop size distribution is completely overwhelmed by relatively small number concentrations of ice particles >100 μm in size. Consequently, liquid water contents computed from the FSSP are considerably less than those measured by either the King or JW probe, but the relative drop size spectra are occasionally useful. Detailed analysis of FORMVAR replicator data taken over Florida (Willis et al. 1994) suggests that on occasion, low LWC of about 0.1 g m^{-3} does exist in regions with substantial ice. Therefore, the low limit of liquid water content for charge separation cannot be ignored but may be difficult to measure. It is pointed out that the FORMVAR replicator technique is the only means whereby droplets and graupel particles can be measured in the *same* air parcel using the same instrument and a sample length of a few meters. Otherwise combining data from two separate 2D probes must rely on a statistical comparison over some kilometer path length and may not distinguish whether the two samples are interacting in a microphysical sense.

Electric fields (**E**) were measured at 1-Hz frequency with a set of four conventional shutter-type mills. These 6-cm diameter field mills are mounted in orthogonal pairs on the fuselage along or near lines of symmetry (Fig. 1). This orientation is important since it allows us to use the sums and differences of the mill outputs to

derive the electric field components in the vertical (E_z, since 1987) and horizontal (E_y, parallel to the wing axis, since 1991), and aircraft charge. The component along the flight track (E_x) is not determined. Correlations of electric field changes caused by lightning discharges cannot be determined with the present low time resolution system, as there is no means to detect and accurately time the occurrence of discharges and lightning flashes. Also, these storms were far out of range of the shore-based lightning detection networks.

Aircraft charge is represented as an equivalent field (A_z and A_y) and the ambient electric field components are computed by summing or differencing the orthogonal field estimates, assumed to be symmetrical at the 0°, 90°, 180°, 270° position. These values provide an estimate of the quality of the **E** measurements. For these purposes, with the aircraft in level flight, a positive vertical field E_z implies negative charge above the airplane and positive (or lesser negative charge) below. Similarly, a positive horizontal field E_y indicates negative charge to the right of the heading and positive to the left. To the extent that these estimates are consistent, the values of E_z and E_y determine on which side of the aircraft the effective charge center is located (Fig. 1). Local electric field strength is increased in the vicinity of the metal aircraft skin; errors in the ambient **E** estimates arise because of errors in the determination of the enhancement coefficients at the mill-mounting locations. In addition, the aircraft does not necessarily charge uniformly over its (painted) surface during flight though ice particles. Our analysis ignores cross-terms between E_x, E_y, and E_z. The WP-3D field mill system gives magnitudes for **E** that we believe are accurate to within a factor of 2 for field components parallel to a measurement direction; additional details are presented in the appendix.

During passes through water cloud ($T > 0$°C), **E** is measured within the limits of uncertainty discussed above and in the appendix. During passes through clouds containing ice particles, the aircraft is charged to very high values, and a question arises in distinguishing between ambient field and aircraft self-charge. Measuring **E** under these circumstances is far from satisfactory, and the measurements given are to be judged considering the consistency between estimates of aircraft charge made with the vertical mills with that obtained from the horizontal mills. We did not try to estimate E_x, the component of the electric field along the flight track. The E_x values are contaminated by plumes of charge streaming off the aircraft in precipitation (Harris-Hobbs et al. 1994; Jones et al. 1993). We point out that our analysis ignores cross components, limiting accuracy to some 10% under some conditions. Also, from the viewpoint of data interpretation, **E** measured just before entry into cloud and precipitation is more reliable than that measured on cloud exit, as iced regions on the aircraft evaporate and break up irregularly. The minimum detectable signal (MDS) for **E** is 1.5 kV m^{-1}, about 15 times the fine weather field.

The 2D particle image data were analyzed with a 6-s averaging period. We inspected the images visually to discriminate between images of ice particles and supercooled water drops. This identification is accurate in the case of images where $D > \sim 0.8$ mm. Raindrop images of this size and larger are deformed into a nearly elliptical shape (Black and Hallett 1986) by the airflow around the 2D probes, whereas graupel and other ice particles show no such distortion. In the case where all particles are smaller than this, graupel and other ice particles have rough edges, whereas drops are smooth-edged. Images were deemed to be all liquid if no obvious ice particles were seen, and all ice if most images were noncircular and the JW LWC < 0.2 g m^{-3}. In case of doubt, images were defined as ''mixed,'' where the smaller particles were assumed to be liquid and the processing program attempted to pick out the ice based upon the circularity of the image. Ice discrimination becomes progressively more difficult as the maximum image dimension drops below about 0.2 mm. If particles have maximum dimensions smaller than this, ice/water discrimination becomes impossible without other aid (such as a JW signal). Times on these data were adjusted to correspond to the center of the averaging period. The cloud probe (2D-C) records images from 0.05 to 1.6 mm in diameter, the precipitation probe (2D-P) from 0.2 to 6.4 mm. In addition, since the occasional 2D records with anomalously small sample volumes (caused by a variety of electronic problems) can produce unreasonable 6-s average concentrations, all such occurrences were altered manually by recomputing the number concentrations and water contents using the average sample volume from the two adjacent 6-s averages.

5. Hurricane flights

Data obtained near the melting level and higher in or near the eyewall in two hurricanes form the bulk of the data presented here. All of the significant electrification was associated with convection. The first of these storms (Hurricane Claudette, 8 September 1991) contained strong updrafts and strong **E**; the other one (Hurricane Tina, 29 September 1992) had weaker updrafts and little noticeable electrical activity. Unless otherwise noted, all of the observations reported here occurred during daylight. Another hurricane mentioned is Atlantic basin Hurricane Emily (1987), a storm with exceptionally strong vertical winds (Black et al. 1994). Storms with weak updrafts and weak electric fields include Hugo on 21 September 1989 (all night passes) and Gustav (1991). Table 1 lists hurricane penetrations through 1995 where visual observations of lightning were made (by the appropriate scientist, who also questioned crew members). These observations are particularly interesting in case of a *lack* of lightning observation during night flights

TABLE 1. Summary of lightning/electric field dataset at the Hurricance Research Division. Flight date is in column 1, storm name is in column 2, cloud LWC devices available are in column 3, column 4 is a judgment about the 2D probe data quality, column 5 indicates the field mills used, and column 6 is for comments. In the storm name, ''D'' signifies a daylight flight and ''N'' a night flight. Some flights had both daylight and night portions. A ''??'' in column 4 indicates that those data have not been examined. Field mill abbreviations are up (U), down (D), right (R), and left (L). Aircraft designations are *NOAA-42* (H) and *NOAA-43* (I).

In-situ electric field/lightning data in hurricanes					
Flight ID	Storm name	Cloud LWC	2D images	Field mills	Comments*
840909I	TS Diana (N)	JW, FSSP	sparse	—	Electrified outer band
860921H	Newton (D/N)	JW, FSSP	good	D only	Melting level
860930H	Paine (D/N)	JW, FSSP	good	D only	
870922H	Emily (D)	JW, FSSP	good C, P	U, D	Electrified eyewall, ±20 m s^{-1} vertical wind, 5–6-km JW broke 2104:00
870929H	Ocean Cu. (D)	FSSP	good	U, D	
870930H	Ocean Cu. (D)	FSSP	good	U, D	
880914H	Gilbert (N)	JW	none	U, D	3-km LTM
880916H	Gilbert (N)	JW	none	U, D	3-km LTM
890805I	TS Dean (D)	JW, FSSP	sparse	U, D	
890903I	Gabrielle (D/N)	JW, FSSP	sparse	U, D	
890921I	Hugo (N)	JW	none	U, D	3 km
891014I	Jerry (D)	JW	none	U, D	Landfall
900827I	Gustav (D)	JW, FSSP	good	U, D	3-km LTM
900828I	Gustav (D)	JW, FSSP	good	U, D	3-km LTM
900829I	Gustav (D)	JW, FSSP	good	U, D	3-km LTM
900830I	Gustav (D)	JW, FSSP	good	U, D	3-km LTM
900831I	Gustav (D)	JW, FSSP	good	U, D	3-km LTM
900919I	TD-11 (D)	JW	none	U, D	3-km LTM
900921I	TD-11 (D)	JW	none	U, D	3-km LTM
900928I	Ocean Cu. (D)	JW, FSSP	sparse	U, D	
910907I	Claudette (D)	JW, FSSP	good	U, D, L, R	3-km eyewall study
910908I	Claudette (D)	JW, FSSP	spotty	U, D, L, R	Electrification. Supercell numerous strikes, JW broke ~1800:00
910923I	Jimena (D/N)	JW	none	U, D, L, R	3-km eyewall evolution
910924I	Jimena (D/N)	JW, FSSP	??	U, D, L, R	3-km eyewall evolution
920929I	Tina (D)	JW, FSSP	good	U, D, L, R	Electrification weak convection
930827I	Emily (D)	JW	none ?	U, D, L, R	ODW, 6 km
930828I	Emily (D)	JW	none	U, D, L, R	ODW, 6 km
930829I	Emily (D)	JW	none	U, D, L, R	ODW, 6 km
930928I	Ocean Cu. (D)	JW	none ?	U, D, L, R	
930930I	Ocean Cu. (D)	JW, FSSP	good C, P	U, D, L, R	Some good convection
940820I	T.S. Chris (D)	JW, FSSP	??	U, D, L, R	Cyclogenesis, 500 mb
940910I	T.S. Debby (D/N)	JW, FSSP	??	U, D, L, R	Genesis, 500-mb ''frequent lightning''
940911I	Debby (D/N)	JW, FSSP	??	U, D, L, R	Genesis, 500 mb
940924I	Olivia (D)	JW, FSSP	good C, med. P	U, D, L, R	4–5-km eyewall evolution (VME)
940925I	Olivia (D)	JW, FSSP	good C, med. P	U, D, L, R	4–5-km VME
941112I	T.S. Gordon (D)	JW, FSSP	sparse	U, D, L, R	NHC Reconnaissance
941113I	Gordon (D)	JW, FSSP	sparse	U, D, L, R	NHC Reconnaissance
950801I	Erin (D, N)	JW, FSSP	good C, med. P	U, D, L, R	3-km NEXRAD radials
950815I	Felix (D, N)	JW, FSSP	??	U, D, L, R	ODW 4–500 mb
950816I	Felix (D, N)	JW, FSSP	??	U, D, L, R	ODW, EFM calib. 2053 *Z*, Fig. 4 1940*Z* ff
950827I	Iris (D/N)	JW, FSSP	??	U, D, L, R	4-km VME
950828I	Iris (D/N)	JW, FSSP	??	U, D, L, R	4-km VME; lightning 2323 *Z*
950904I	Luis (N)	JW, FSSP	??	U, D, L, R	500-mb VME; fix 0051 *Z*, 0259 *Z*
950907I	Luis (D/N)	JW, FSSP	??	U, D, L, R	4-km vortex dynamics (XCDX)
950929I	S. Fla. (D)	JW, FSSP	2 2D-P's	U, D, L, R	Low-altitude clouds and climate
951094I	Opal (D)	JW, FSSP	good C, P	U, D, L, R	5-km NEXRAD radials

* Abbreviations for hurricane field program activities:

EMF - Electric field mill
Genesis, Cyclogenesis - Tropical cyclogenesis experiment
LTM - Long-term monitoring
Landfall - Tropical cyclone windfields at landfall experiment
ODW - Hurricane synoptic flow experiment
VME - Vortex evolution experiment
XCDX - Extended cyclone dynamics experiment
Electrification - Hurricane electrification experiment

in Hugo. Of the storms listed in Table 1, our most comprehensive dataset is from Hurricane Tina. No 2D image data are available from Hurricane Hugo; in Claudette, 2D data are unavailable from the start of the first penetration at 1613:00 (all times are UTC) to about 1950:00, and after 2324:53 because of equipment failures. No cloud liquid water content data are available from Claudette because the JW and King LWC sensors were both damaged by graupel impacts on the first pass through the eyewall.

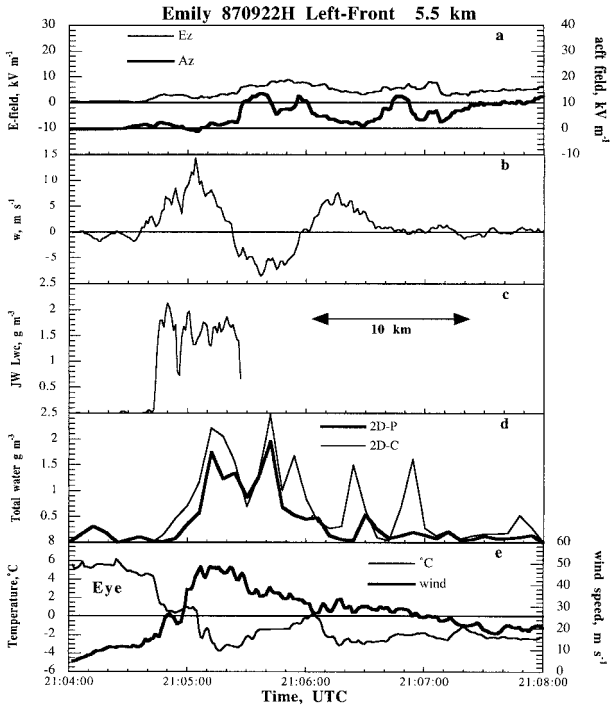

FIG. 2. Flight-level data from a left-front quadrant eyewall pass in Hurricane Emily, 22 September 1987. In this and all subsequent figures, the quadrant is referenced to the storm motion. (a) Vertical electric field and aircraft field (k V m^{-1}); (b) vertical velocity, (m s^{-1}); (c) cloud liquid water content from the JW probe (g m^{-3}); (d) total water content (liquid plus ice) deduced from 2D particle image data; (e) air temperature (°C) plus horizontal wind speed (m s^{-1}). In this and all subsequent flight-level data figures, the eye (and warmest temperature) is on the left-hand side of the plot. A lightning flash struck the aircraft at about 2105:40.

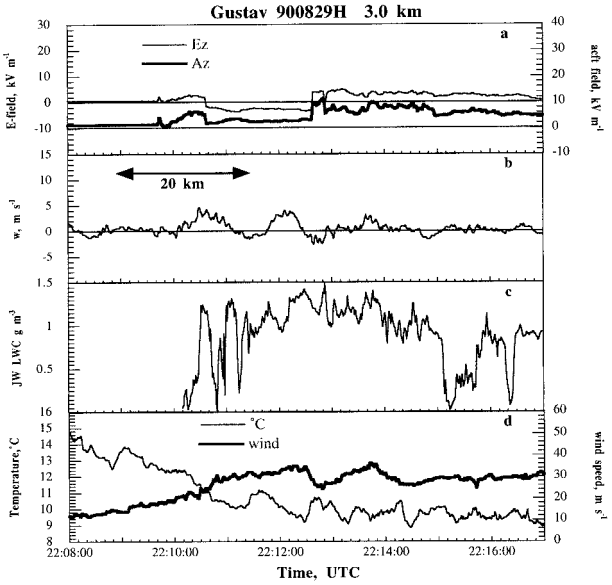

FIG. 3. Flight-level data from Hurricane Gustav, 29 August 1990. (a) Vertical electric field E_z and aircraft field A_z (kV m^{-1}); (b) vertical velocity (m s^{-1}); (c) cloud liquid water content (JW) (g m^{-3}); (d) temperature (°C) and wind speed (m s^{-1}).

The first hurricane in which we measured **E** (E_z only) was a daylight flight into Hurricane Emily on 22 September 1987. This storm was a ''rapidly deepening'' storm, and it contained the strongest flight-level vertical winds (updrafts and downdrafts in excess of 20 m s^{-1}) ever observed in any tropical cyclone (Black et al. 1994). Eyewall penetrations were made in a symmetric pattern about the eye to obtain the maximum areal coverage for the radar. All portions of the eyewall were sampled, but an unresolved calibration problem rendered the exact magnitude of these fields (Fig. 2a) uncertain. Lightning (a good indicator of local electrical activity) apparently struck the aircraft at about 2105:50 during the pass shown. Like most of the passes through Emily, this pass (outside the eyewall) was just above the melting level at an altitude near 5.0 km. Three lightning strikes on the WP-3D aircraft (out of a total of nine flashes observed) were noted by the flight crew; all three of these strikes occurred in the left-front quadrant of the storm. Here, strong (>10 m s^{-1}) updrafts containing cloud water and millimeter raindrops but no graupel were adjacent (within a few hundred meters) to downdrafts containing millimeter diameter graupel, raindrops, and cloud water.

Hurricane Gustav on 29 August 1990 was the first time that both the electric field mills and the 2D probes simultaneously performed adequately. At the time of this flight, Gustav had an asymmetric eye open on the southeast side and was located near 25°N, 58° W, ~800 km southeast of Bermuda. No lightning was observed any time during this daylight mission; peak electric field strength (Fig. 3a) was <10 kV m^{-1}, and peak vertical velocities (Fig. 3b) were always <5 m s^{-1}. The pass shown penetrated the strongest portion of the eyewall and is labeled ''leg 3'' in Fig. 4 of Gamache et al. (1995). This was a typical pass through the strongest convection of this storm. These conditions represent the case of the weakly electrified storm. It should be noted, however, that the aircraft never flew above the melting level where charge separation may have been occurring.

A night flight through Hurricane Hugo on 21 September 1989 presented us with an opportunity to obtain qualitative data in a land-falling hurricane. This storm's convection had weakened considerably, its eye was much larger, and its sustained winds were weaker (but still substantial) than it was on 17 September when it struck eastern Puerto Rico (Case and Mayfield 1990). Visual observations by one of us (JH) over a 3-h period during a night flight failed to reveal any lightning at all within 100 km of the eyewall.

Hurricane Claudette on 8 September 1991 exhibited significant electrical activity within its eyewall. On this day, Claudette was about 220 km southeast of Bermuda moving north at 7 m s^{-1} (Pasch and Avila 1992). The eyewall was incomplete (Fig. 4) and dominated by a

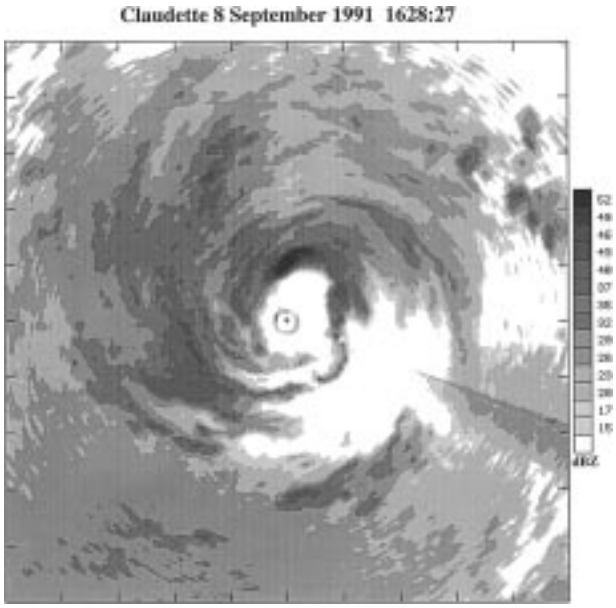

FIG. 4. Single-sweep PPI map of Hurricane Claudette at 1628:27. North is toward the top of the figure. The aircraft penetrated the storm along a northwest–southeast track. The strong convective cell in which the strongest **E** and most lightning flashes were encountered is in the north eyewall. In this and all subsequent radar images, the aircraft position at the time the image was obtained is marked with a +. The blanked-out area around the + is caused by the range delay of the radar, and the ring of return around the + is where the sidelobe return from the sea surface appears.

vigorous convective cell with radar reflectivities exceeding 50 dB*Z* on the north side. The most intense electrical activity occurred in and near this cell. On each of the first three penetrations of this cell, the aircraft was struck by lightning, events that caused equipment failures and data losses. Thereafter, the pilots refrained from penetrating that area.

The WP-3D made repeated radial penetrations of the northwest eyewall of Claudette at various altitudes from 4.5 to 7.0 km at temperatures between +2° and −13°C. These penetrations passed through or near the strongest reflectivity area. Unlike other hurricane research flights, the pilot avoided the center of the strongest radar reflectivity (>50 dB*Z*) area in the eyewall after the first few passes because of danger of excessive lightning strikes and the impacts of small hail.

Hurricane Tina was observed when it was located in the eastern Pacific Ocean about 1400 km west of Puerto Vallarta, Mexico, on 29 September 1992. The storm convection was more widespread and vigorous at the start of the penetrations than it was at the end, and no lightning was observed visually. Our data were obtained primarily in the northeast portion of the storm at temperatures ranging from +5° to −15°C. In this storm, the areas with the strongest radar reflectivity were specifically selected for study, as opposed to simply making passes based on geometric considerations (to ensure complete radar coverage of the entire storm, for example). Tina's strongest radar reflectivities were not as persistent or reflective as those of Claudette.

In the discussion that follows, the (radial) passes are grouped by the temperature instead of by storm. When the temperature level of a radial pass is given, we use the temperature in the stratiform area outside the eyewall (usually several degrees cooler than the eye). In these penetrations, the warmest temperatures indicate the direction to the storm center, and the data are plotted such that the eye is always on the left side of the graph. We chose to group the flight-level data in this manner because both laboratory and field studies (e.g., Reynolds et al. 1957; Takahashi 1978; Saunders et al. 1991; Brook et al. 1980) show that liquid water content and temperature are the most important variables governing the rate at which charge can be separated in a cloud. Further, passes made at a given temperature were more similar between storms than they were to passes within the same storm, but at different temperatures.

a. Passes at altitudes lower than the −5°C isotherm

These passes were made in regions with updrafts carrying supercooled cloud water aloft on the inner edge of the eyewall, and ice-containing downdrafts farther from the center. Tina pass 2 (Fig. 5) from 2224:00–2236:00 was made at the +2°C level. At the time of this pass, the storm (Fig. 5 radar) was attempting to form a concentric eye (Willoughby et al. 1982). The strongest convection and electric field (**E**) occurred in the outer convective ring. These fields (Fig. 5a) were observed in a weak downdraft on the cold side of the secondary wind maximum well outside the radius of maximum wind (RMW; on the left side of Fig. 5f). In this instance, E_z went sharply positive, reaching a maximum in the downdraft on the outer edge of the updraft, and decreased slowly as the aircraft penetrated the updraft. Cloud liquid water as measured by the JW device (Fig. 5c) in the region where the most rapid change in **E** occurred was about 0.25 g m^{-3} or less. The ''top hat'' JW profile in the updraft from 2229:00 to 2230:50 is the result of a problem with the probe, not the actual peak cloud LWC. Because of corroded electrical connections on the JW probe, the measured cloud LWC did not exceed about 0.8 g m^{-3}. An additional indication of cloud LWC in this updraft is the temperature decline (Fig. 5f) from about 2229:00 to 2230:50. We attribute this temperature response to cooling caused by the impact of cloud droplets on the Rosemont temperature sensor (Lenschow and Pennel 1974). The strong excursions in **E** observed near 2229:00 were coincident with an area that contained melting ice particles advected from above and upstream. At the RMW (2231:00), the small **E**s occurred in a weak downdraft, but in a region that contained only liquid.

Melting-level passes were made in both Tina and Claudette. Tina pass 3 (Fig. 6, about 2244:00–2252:00) illustrates the usual features of these passes. At the time

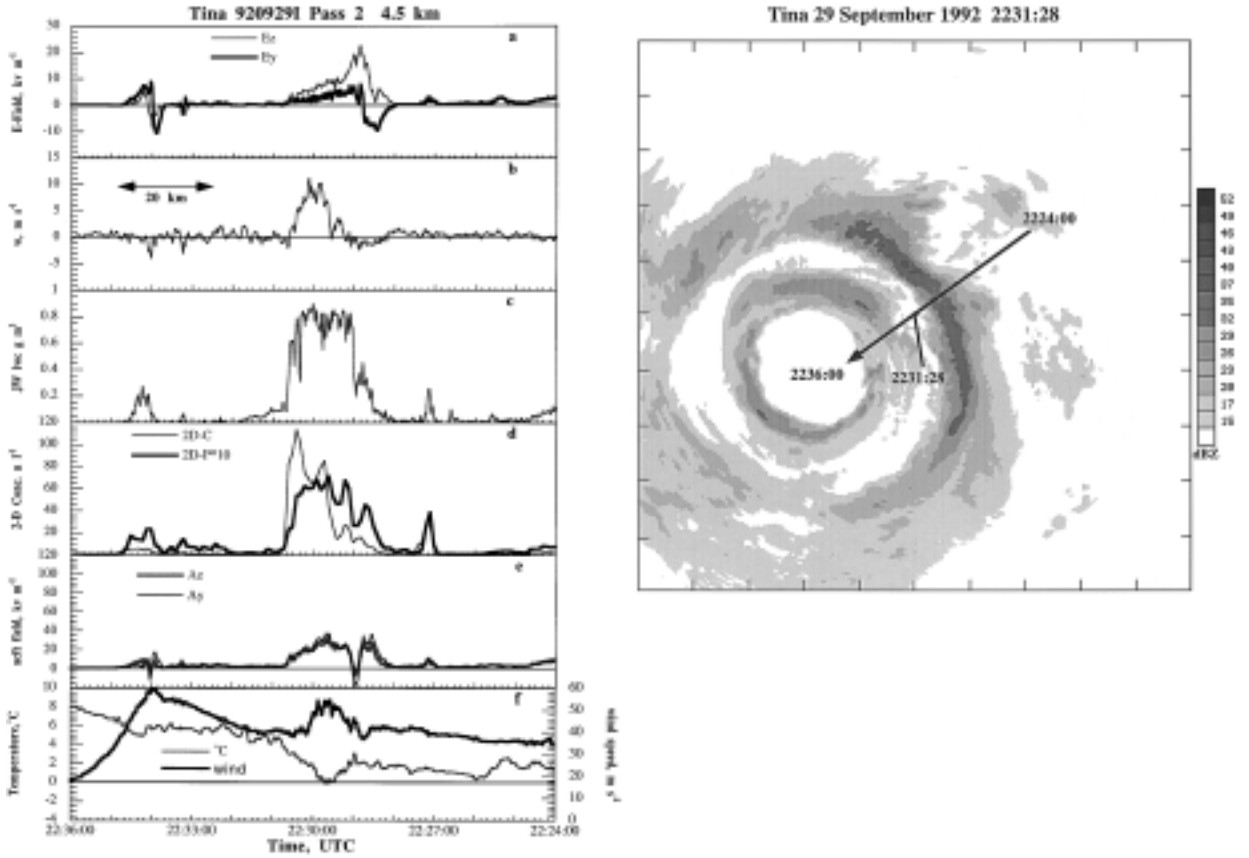

FIG. 5. Flight-level data from Hurricane Tina, 29 September 1992, from the inbound 4.5-km altitude (+2°C) pass from 2224:00 to 2236:00. (a) Vertical (E_z) and horizontal (E_y) **E** components (kV m^{-1}); (b) vertical velocity (m s^{-1}); (c) cloud liquid water content from the JW probe (g m^{-3}); (d) particle number concentration (L^{-1}) deduced from 2D particle image data. The precipitation probe number concentration is multiplied by 10 for clarity. (e) Vertical and horizontal aircraft field (kV m^{-1}) from both pairs of field mills; (f) temperature and horizontal wind speed. (Radar) Single-sweep PPI reflectivity display from the WP-3D lower fuselage radar. The start and end points of the pass are as shown by the long arrow. The aircraft position at the time of the radar image is marked.

of this pass, the strongest reflectivity in the outer convective band was upstream from the flight track (Fig. 6 radar). As the aircraft penetrated the outer band updraft (Fig. 6b) at 2245:50, the horizontal field E_y started positive but switched to negative immediately upon entering an area that contained mixed-phase particles at 2247:10 (Fig. 6a). This behavior suggested that predominantly negatively charged particles were advecting from the more strongly reflective area upstream (the right of the aircraft) at this location. Here E_y indicated that positive charge was on the left side of the aircraft track as the cloud LWC (Fig. 6c) observed by the JW decreased to about 0.4 g m^{-3}. Most of the JW LWC observed after 2247:20 is attributable to the impact of ice particles (Fig. 6d) on the JW sensor; we have often noted this behavior of the JW in hurricanes (e.g., Black et al. 1994) where the vertical velocity is near zero in the presence of copious aggregated ice at temperatures near −2°C. By 2248:10 E_y diminished to MDS, indicating that the charge was uniform on both sides of the aircraft.

The magnitude of E_z gradually increased in the updraft in rain and peaked in the cold side downdraft, suggesting a negative charge center at or above flight level. The polarity of E_z (Fig. 6a) also fluctuated outside the updraft in the mixed-phase region, indicating mostly net negative charge above flight level, positive (or no) charge below, in a region containing mostly (melting) ice particles. Doppler radar scans (not shown) suggest that these particles were simply falling from higher, colder cloud upstream, rather than being brought down in a strong downdraft. After 2248:40, **E** diminished to MDS in aggregated ice.

The lowest-level pass in Claudette (Fig. 7) penetrated the storm from the north at 4.5 km, did not encounter any strong updraft, and showed little electrical activity. Outside the eyewall, the E_z component (Fig. 7a) was strongest, showing positive values (negative charge aloft and/or positive below) at virtually all times. These electric fields occurred both in areas with mixed-phase hydrometeors (Fig. 7c) consisting predominately of (melting) irregular shaped ice particles and a few water drops, and in an area that had no ice particles. However, the peaks in the E_z component were reasonably well correlated with peaks in the 2D-P probe ice concentration.

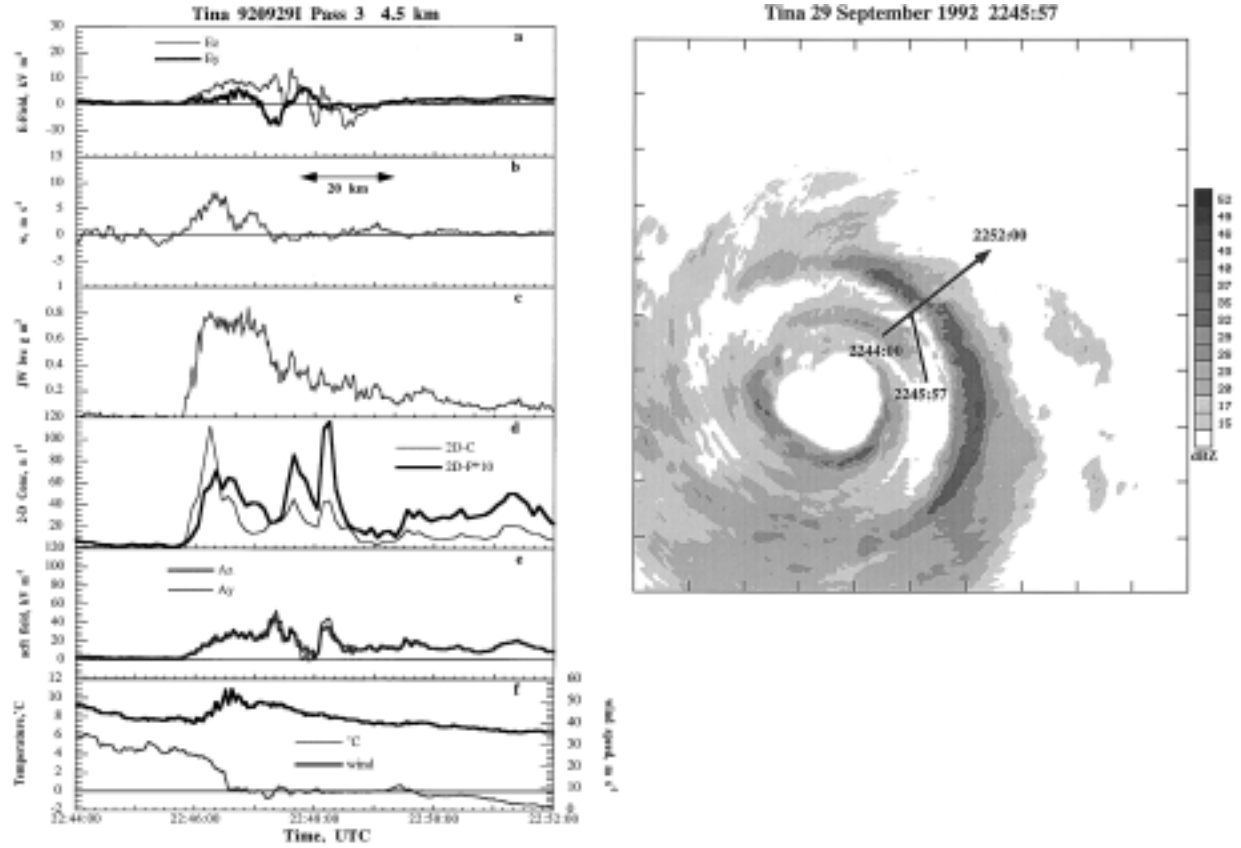

FIG. 6. As in Fig. 5 but for the reciprocal outbound pass from 2244:00 to 2252:00 (0°C). (a) Vertical (E_z) and horizontal (E_y) **E** components (kV m^{-1}); (b) vertical velocity (m s^{-1}); (c) cloud liquid water content from the JW probe (g m^{-3}); (d) particle number concentration (L^{-1}) deduced from 2D particle image data. The precipitation probe number concentration is multiplied by 10 for clarity. (e) Vertical and horizontal aircraft field (kV m^{-1}) from both pairs of field mills; (f) temperature and horizontal wind speed. (Radar) Single-sweep PPI reflectivity display from the WP-3D lower fuselage radar. The start and end points of the pass are as shown by the long arrow. The aircraft position at the time of the radar image is marked.

In the eyewall, the strong negative excursion in E_y at 2152:00 and the positive E_z occurred just when large (melting) graupel particles were observed but is also affected by precipitation-induced static charges (Fig. 7d). As in Tina, the negative E_y excursions occurred prior to the E_z peak on the outer edge of the eyewall (Fig. 7 radar). No 2D image data are available from the eyewall to aid in the interpretation of these results.

The Claudette pass at 4.9 km from 2208:00 to 2215:00 (Fig. 8) illustrates the effect of vertical velocity on the electrical and microphysical structure of this eyewall. This twilight pass encountered a strong updraft in a convective cell outside the eyewall reflectivity maximum (Fig. 8 radar), with a peak vertical wind speed of ~9.5 m s^{-1}. The E_z field (Fig. 8a) showed moderate excursions from 2209:00 to 2212:30, with two out of three positive peaks in updrafts collocated with the banded reflectivity relative maxima, negative in downdraft (Fig. 8b) and neutral areas with mostly ice. Liquid water (Fig. 8c) and a few graupel particles coexisted on the edges the updrafts. Note that the most pronounced excursions in E_z occurred on the edges of the updrafts, not in the center. Lightning flashes were observed at about 2209 and/or 2210, but the timing of these flashes is insufficiently precise to relate these to the changes in E_z polarity that occurred at these times. This behavior suggests that (a) the (negative) charge center is located above the aircraft and (b) the most rapid charge separation is taking place in regions of modest cloud LWC in the presence of ice particles, rather than in the LWC maximum, which always occurs at the peak updraft (e.g., Black et al. 1994). At these temperatures, ice particles are only found in the periphery of the updraft. The ~2°C temperature changes at 2210:00 and 2212:30 (Fig. 8e) may be related to the evaporation of liquid water off the sensor in the updraft. The E_y field was consistent with negative charge centered slightly to the left (upwind) of the aircraft in the updraft and no laterally offset charges elsewhere. These E_z polarity variations suggest that the aircraft flew underneath two distinct negative charge centers, one in each updraft. The particle phase was mostly liquid with some millimeter graupel in the positive field areas and mostly graupel with some columnar images in the negative regions. After 2213:00,

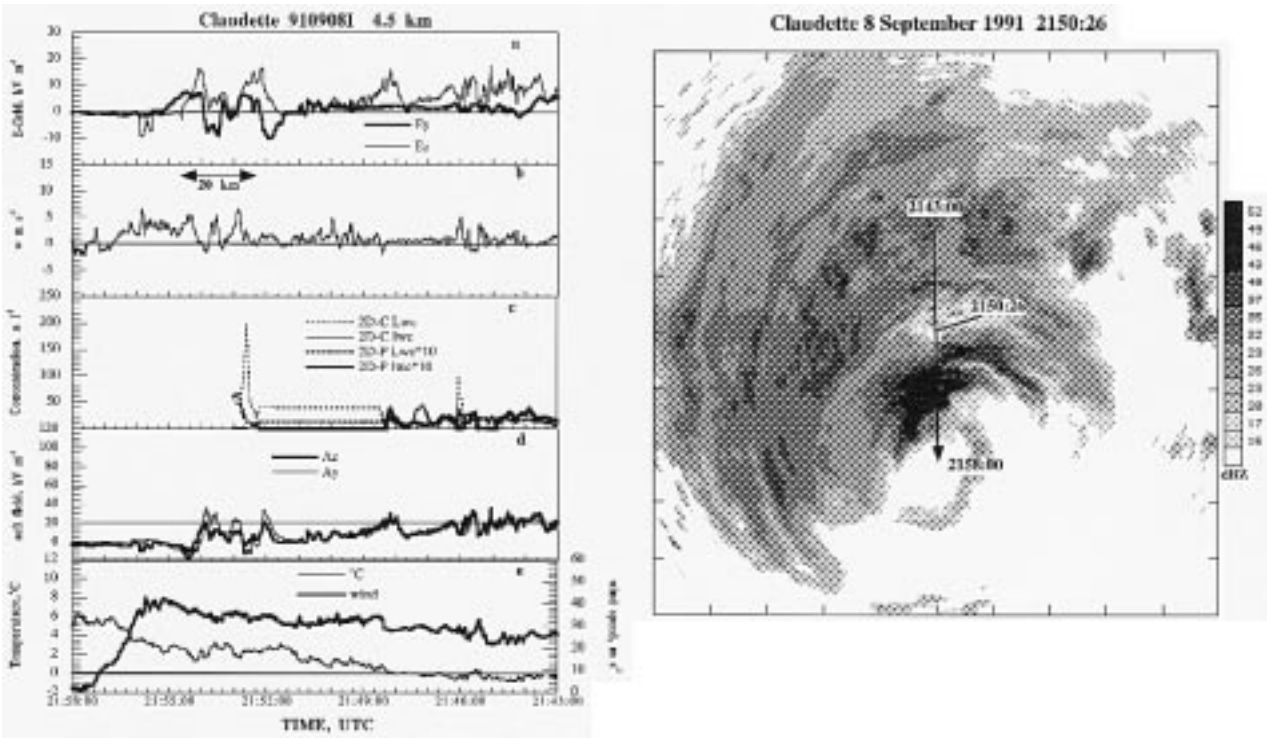

FIG. 7. Flight level data from an inbound pass at 4.5 km (+3°C) in Hurricane Claudette on 8 September 1991. (a) Vertical and horizontal electric field (kV m^{-1}); (b) vertical velocity (m s^{-1}); (c) two-dimensional particle image number concentration (L^{-1}) by particle phase. The 2D-P values are multiplied by 10 for clarity. (d) Vertical and horizontal aircraft field (kV m^{-1}); (e) temperature (°C) and horizontal wind speed (m s^{-1}). (Radar) Single-sweep PPI reflectivity display from the WP-3D lower fuselage radar. The start and end points of the pass are as shown by the long arrow. The aircraft position at the time of the radar image is marked.

most particles were liquid, consistent with the weak **E** observed there.

The inbound pass through Tina from 2300:00 to 2310:00 (Fig. 9) encountered the second strongest (~9 m s^{-1}) updraft of this storm. At this altitude, the outer convective band shows the weak reflectivity (Fig. 9 radar) consistent with an overwhelming abundance of low-density ice. The updraft at 2304:00 (Fig. 9b) occurred in a prominent secondary wind maximum located in the outer convective band ~30 km away from the eyewall. While crossing this rainband from 2302:00 to 2306:00, the aircraft apparently carried unbalanced charge (Fig. 9e), as the A_z and A_y graphs remained in phase, but differed in magnitude. Ice particle types outside the updraft were the usual mixture of rounded, irregular crystals, and columns normally observed at this level in hurricanes. In the updraft, graupel particles up to 3 mm in diameter coexisted with millimeter diameter raindrops and small unidentifiable images. In this pass, E_z (Fig. 9a) was consistently positive (and unremarkable) from 2300:00 through the updraft. Upon exiting the updraft (Fig. 9b), E_z abruptly reversed polarity in an area containing needles, aggregates of needles, and irregular, sharp pointed crystals. These particles had clearly undergone depositional growth at or near water saturation at −5°C, the flight-level temperature. At 2305:40, the aircraft entered a clear area and **E** decayed rapidly. From 2300:00 through 2301:20 E_y was weakly positive, when the JW (Fig. 9c) increased slightly above background.

During this pass, E_y was near zero in the presence of cloud LWC, went slightly negative as the aircraft entered the downdraft, returned to positive in the updraft, and remained with that polarity until the aircraft entered the clear area mentioned previously. A weak excursion in E_z occurred around 2308:00, when the aircraft penetrated the remnant of the inner eyewall at the RMW. The particles encountered there were <1 mm in diameter and consisted of rounded particles, aggregates of small needles, and columns. The lack of significant E_y indicates that the aircraft flew near the charge center.

We note that the apparent JW observed before about 2303:00 is not likely to be true cloud liquid water. Similarly, the large excursion in temperature observed near 2304:00 is not real but is probably related to the impact of supercooled raindrops on the sensor (Willis et al. 1991).

At the 5.7-km level in Claudette after sunset (Fig. 10), multiple lightning flashes were observed both prior to entering the eyewall at about 22:32–22:33, and in cloud at about 22:35; electric fields were encountered almost immediately upon entering the eyewall. The strongest E_z fields (~24 kV m^{-1}, Fig. 10a) during this outbound pass occurred within the high-reflectivity zone

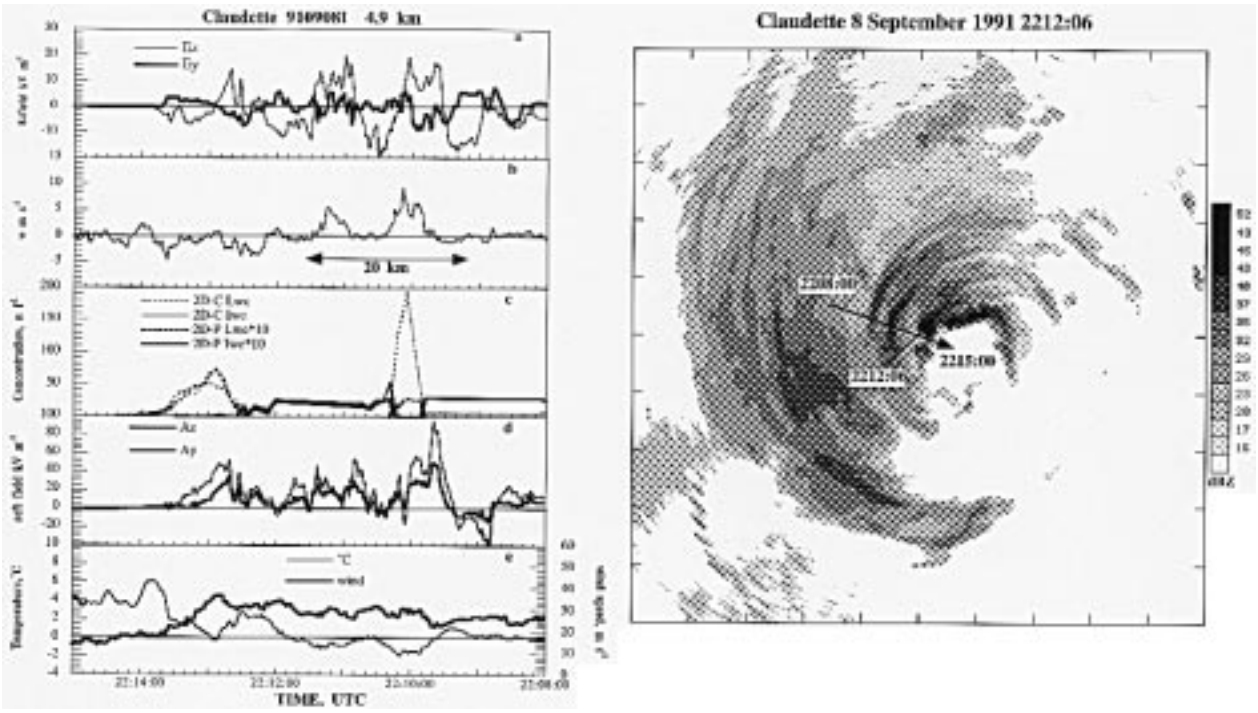

FIG. 8. As in Fig. 7 but for the 4.9-km (+2°C) inbound pass from 2208:00 to 2215:00. Sunset occurred at 22:10:00, and lightning flashes were observed at ~2209 and ~2210. (a) Vertical and horizontal electric field (kV m^{-1}); (b) vertical velocity (m s^{-1}); (c) two-dimensional particle image number concentration (L^{-1}) by particle phase. The 2D-P values are multiplied by 10 for clarity. (d) Vertical and horizontal aircraft field (kV m^{-1}); temperature (°C) and horizontal wind speed (m s^{-1}). (Radar) Single-sweep PPI reflectivity display from the WP-3D lower fuselage radar. The start and end points of the pass are as shown by the long arrow. The aircraft position at the time of the radar image is marked.

downstream from the reflectivity maximum (Fig. 10 radar) in areas with many large (3–6-mm diameter) graupel particles and temperatures near ~−5°C. Note that there are no electric fields observed until most of the particles become ice at $T < 0$°C, and there are no negative E_z values. All of the E_z peaks occurred in relatively weak vertical velocity extrema (Fig. 10b), the first two in the eyewall coincident with updrafts of ~5 m s^{-1}, the other in a ~4 m s^{-1} downdraft containing small ice and large graupel. The negative E_y values before 2235:00 peaked almost in phase with the positive excursions in E_z, and the polarity abruptly reversed within the updraft starting at 2235:10. The 2D-P data are of poor quality, resulting in a severe degradation of the sample volume, but the occurrence of large graupel and rounded ice is correlated with the positive E_z excursions. These data indicate that small particles are nearly absent and that large particles carry more charge. After 2236:30, in a zone without evidence for liquid water and containing rounded particles, large aggregates, and columns, all electric field components were weak and nearly constant, except the minor E_y peak at 2238:00. This peak was correlated with a peak in the 2D-C concentration, and the particles responsible for the concentration peak were small (<0.5 mm long) needles.

b. Passes at altitudes higher than the −5°C isotherm

The higher and colder the aircraft flew in these storms, the more uniform the charging situation became. An outbound pass (in darkness; sunset occurred at 2220:00) at 6.4 km in Claudette (Fig. 11) illustrates this point. This pass penetrated the upwind edge of a ~45-dBZ reflectivity core (Fig. 11 radar) in the eyewall. In the strong updraft near 2319:40 (Fig. 11b), 2D-P image data revealed copious large graupel and evidence of supercooled water where E_z (Fig. 11a) had a substantial positive component. There was also a very strong temperature gradient (Fig. 11e) within this draft; the entire pass was colder than 0°C; the inner edge was at −6°C while the outside was at −12°C. The 2D-P probe malfunctioned at 2320:00; few images of the largest particles exist after this time. Here, the extreme positive excursions of E_z were associated with copious (Fig. 11c) small columns and needles mixed with larger (1–2-mm diameter) rounded particles; When these particles were present E_z was strongest and positive, and nearly zero (or negative) when the larger rounded particles were absent and the small ones were relatively few. Usually E_y was negative, except near the center of the updraft, when it was about zero. These data suggest that the charge center was above and offset to the left of the

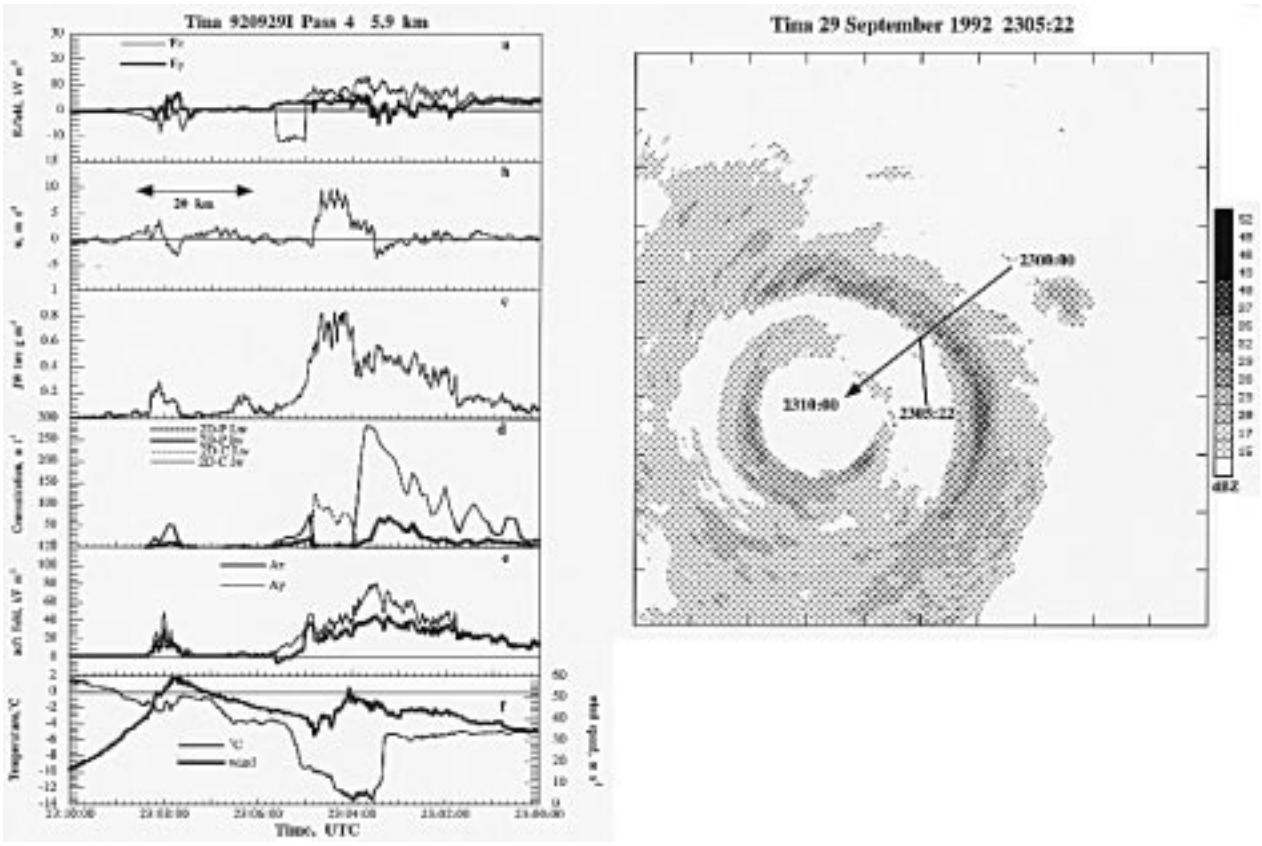

FIG. 9. As in Fig. 5 but for the 5.9 km (−4°C) inbound pass in Tina from 2300:00 to 2310:00. (a) Vertical (E_z) and horizontal (E_y) **E** components (kV m^{-1}); (b) vertical velocity (m s^{-1}); (c) cloud liquid water content from the JW probe (g m^{-3}); (d) particle number concentration (L^{-1}) deduced from 2D particle image data. The 2D-P particle image number concentrations are not scaled. (e) Vertical and horizontal aircraft field (kV m^{-1}) from both pairs of field mills; (f) temperature and horizontal wind speed. (Radar) Single-sweep PPI reflectivity display from the WP-3D lower fuselage radar. The start and end points of the pass are as shown by the long arrow. The aircraft position at the time of the radar image is marked.

track. This pass illustrates the importance of cloud liquid water, since we expect that the cloud liquid water content is greatest in the updraft and least outside it in the presence of so many ice crystals. The 2D-C probe number concentration (Fig. 11c) rose to several hundred per liter, approximately in step with the occurrence of the needles and the positive excursions of E_z. The first (and strongest) of the strong positive E_z values occurred at −6°C in the updraft; the rest were observed at −12°C, but no images of large graupel or evidence of cloud LWC were recorded. Instead, the area contained a weak downdraft that contained primarily very small particles of irregular shape, needles, and columns in concentrations of several hundred per liter (Fig. 11c). These observations indicate that the negative charge center was above and slightly to the left (downwind) of the aircraft within the eyewall updraft.

The highest altitude and coldest pass in Claudette (Fig. 12) was at night at an altitude of 7 km. This pass skirted just upstream from the most reflective cell in the eyewall (Fig. 12 radar), passing this feature on the right side of the aircraft. The strongest updraft in this storm for which we have electric field data (Fig. 12b) was encountered inward of the strong cell, and E_z (Fig. 12a) was always positive. Again, E_z and E_y showed that the aircraft was below and upwind from the apparent charge center located in the direction of the strongest reflectivity. Little 2D-C and no 2D-P image data are available for this pass; those data show only that large (2–8-mm diameter) graupel occurred in the updraft at 2331:00–2331:00, where E_z was most strongly positive. This pass exhibited more precipitation static than the others, as indicated by the separation of the A_z and A_y plots (Fig. 12c). This divergence of the A_z and A_y plots reveals the presence of unbalanced static charges on the aircraft, which is probably the result of asymmetric airframe charging caused by ice particle impacts. Thus, **E** measurements are most suspect between 2328:00 and 2332:00. In spite of this, at 2331:35 the separation of A_z and A_y was at a minimum and E_z was near its maximum, 27 kV m^{-1}, which lends credence to the field measurements in the updraft. Nevertheless, the E_y values consistently point at the nearby reflectivity maximum on the right side of the aircraft as the charge center.

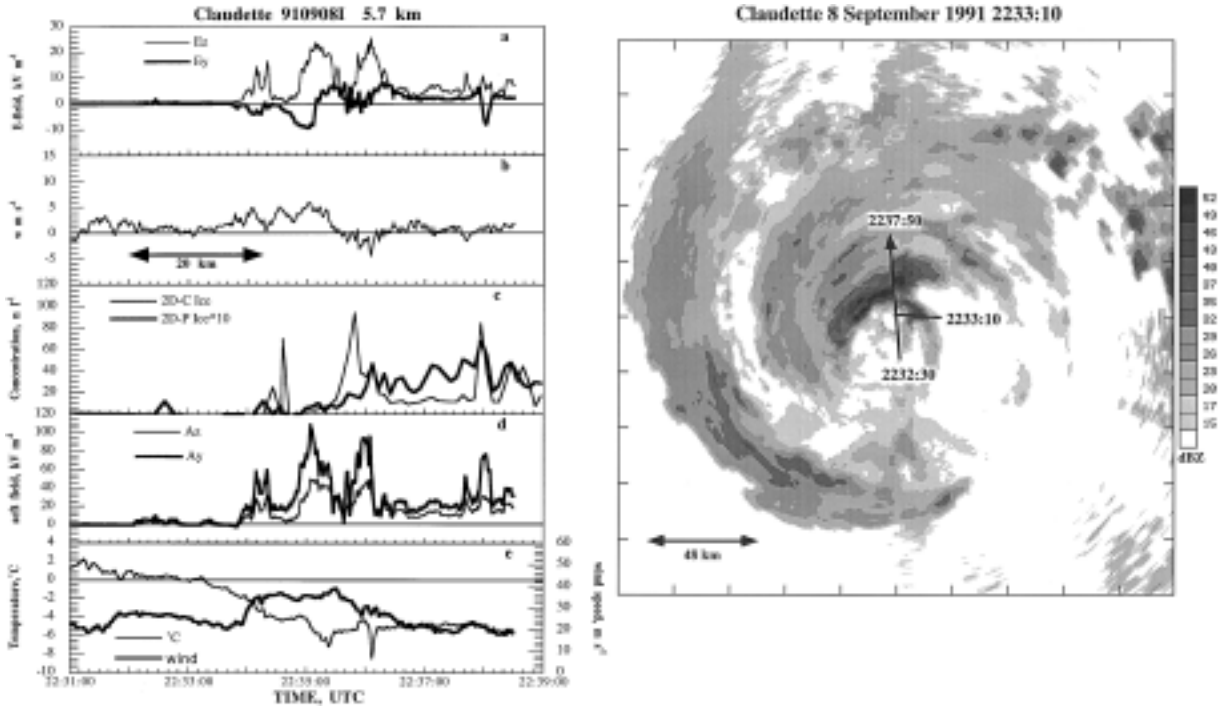

FIG. 10. As in Fig. 8 but for the outbound (night) pass in Claudette at 5.7 km (−5°C) from 2231:00 to 2239:00. Multiple lightning flashes were observed from about 2233–2235. (a) Vertical and horizontal electric field (kV m^{-1}); (b) vertical velocity (m s^{-1}); (c) two-dimensional particle image number concentration (L^{-1}) by particle phase. The 2D-P values are multiplied by 10 for clarity. (d) Vertical and horizontal aircraft field (kV m^{-1}); temperature (°C) and horizontal wind speed (m s^{-1}). (Radar) Single-sweep PPI reflectivity display from the WP-3D lower fuselage radar. The start and end points of the pass are as shown by the long arrow. The aircraft position at the time of the radar image is marked.

Tina passes 5 (Fig. 13) and 6 were the coldest passes we made in that storm. On the outbound pass through the outer convective rainband (Fig. 13 radar), the aircraft encountered a narrow 10 m s^{-1} updraft (Fig. 13b). This updraft was the strongest we encountered in Tina and was similar in peak magnitude to those in Claudette. However, **E** values (Fig. 13a) were weak, the high-velocity core was considerably narrower, and the 6–8-mm diameter graupel particles were not present. The usual 1–3-mm diameter rounded graupel images were observed in the updraft, which was flanked on both sides by areas dominated by columns, needles, and combinations of these. In this instance, the greatest cloud LWC (in the strongest part of the updraft) coincided with the weakest E_z. The cloud LWC (Fig. 13c) is probably good until 2322:40, when the aircraft left the updraft and the sensor responded to ice particle impacts. Both passes were also plagued by disparate A_z and A_y resulting from irregular charges (Fig. 13e) on the aircraft. However, since the changes in A_z and A_y remained in phase, we believe that the relative changes in E_z and E_y are valid. In this instance, in the updraft maximum, E_z dipped just when the difference between A_z and A_y was least and JW LWC was greatest.

Tina pass 6 (Fig. 14) followed a reciprocal path from pass 5 at nearly the same altitude (Fig. 14 radar). In the few minutes that elapsed since the previous pass, the area of the 32–35-dBZ echo decreased and advected farther downwind. Unlike pass 5, a modest ~5 m s^{-1} updraft (Fig. 14b) was encountered in the outer convective band, and the remnant of the eyewall contained mostly downdraft. Although no part of this pass contained **E** > 15 kV m^{-1}, the area with the strongest **E** at this time was the eyewall edge near 2337:00, rather than the major convective band that produced the secondary wind maximum shown earlier. The component E_z (Fig. 14a) was positive all the time, with the strongest fields in areas containing small rounded ice, columns, and needles. The particle type and apparent image density (the ratio of light to shadow within an image's perimeter) increased from 2330:00 until the updraft at about 2332:00. The particle types included irregular particles plus plates with broad branches, columns, and needles. As the aircraft approached the updraft (Fig. 14b), the E_z component (Fig. 14a) gradually strengthened, and the particle mix changed to predominantly rounded ice particles, small columns, and a few irregular particles. In the outer band remnant, the strength of the vertical electric field was related more to the mere presence (or absence) of cloud liquid water from the JW and 2D-P number concentration than anything else. In the eyewall remnant at 2335:00, the peak E_z occurred in a region containing moderate quantities of millimeter diameter rounded particles and small columns. Through-

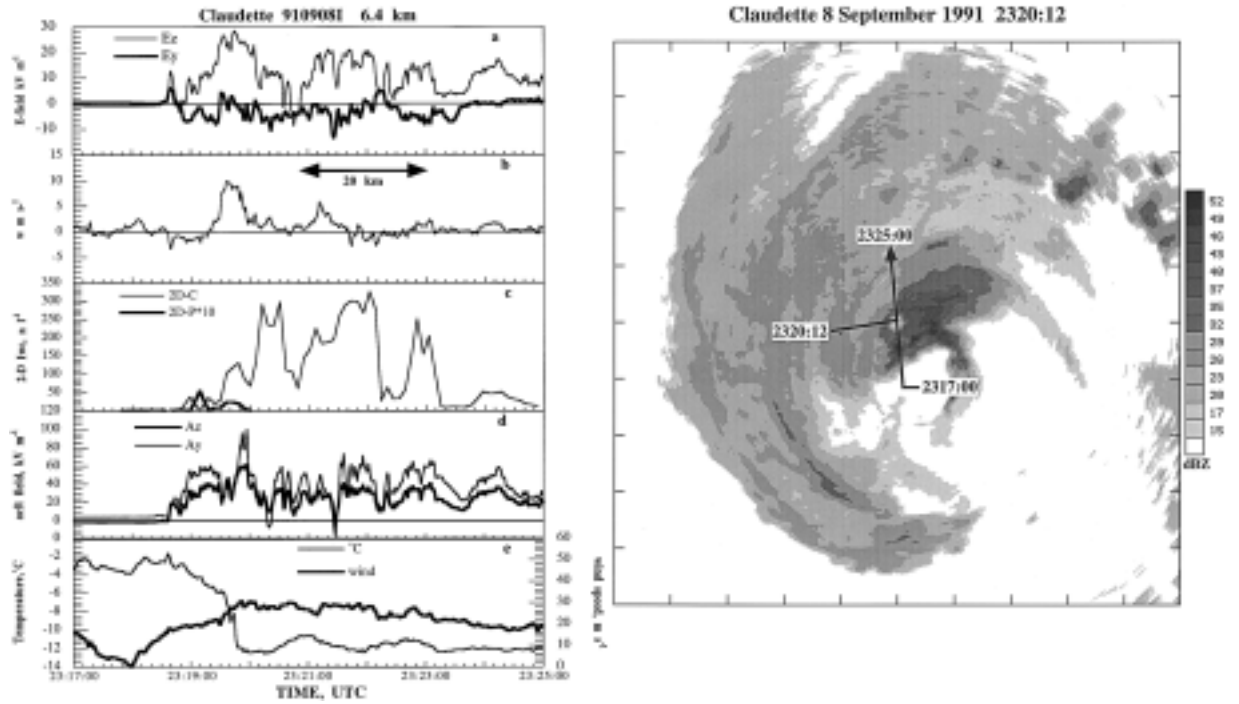

FIG. 11. As in Fig. 10 but for the 6.4-km (−11°C) outbound pass in Claudette from 2117:00 to 2325:00. (a) Vertical and horizontal electric field (kV m^{-1}); (b) vertical velocity (m s^{-1}); (c) two-dimensional particle image number concentration (L^{-1}) by particle phase. The 2D-P values are multiplied by 10 for clarity. (d) Vertical and horizontal aircraft field (kV m^{-1}); temperature (°C) and horizontal wind speed (m s^{-1}). (Radar) Single-sweep PPI reflectivity display at 2325:00 from the WP-3D lower fuselage radar. The start and end points of the pass are as shown by the long arrow. The aircraft position at the time of the radar image is marked.

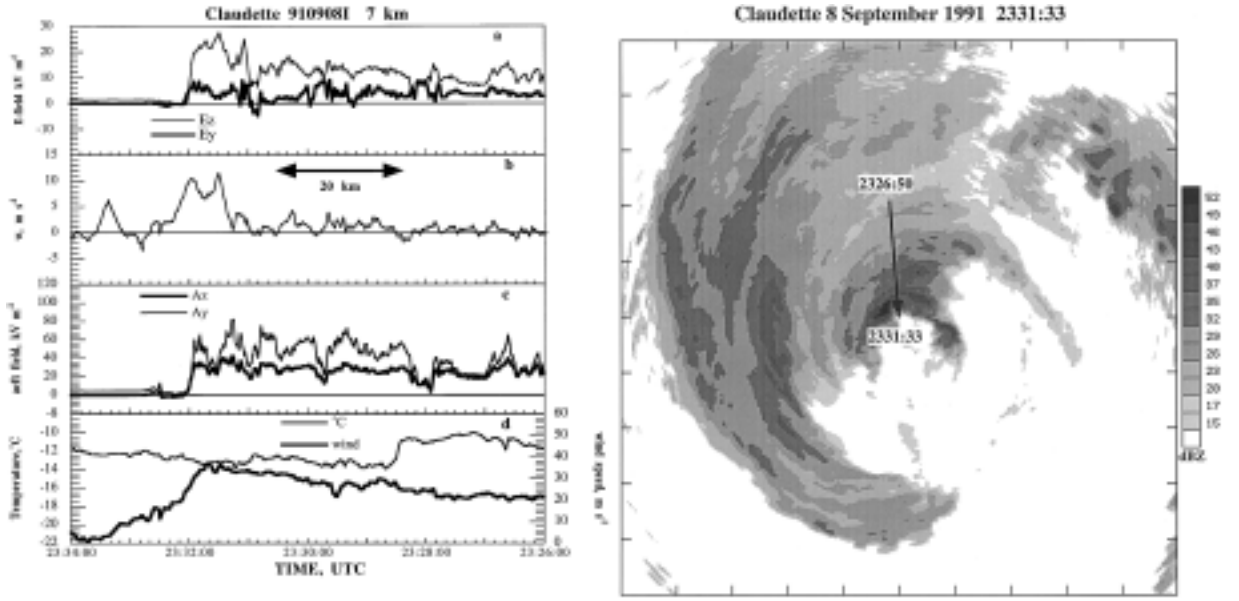

FIG. 12. Flight level data from the 7.0-km (−13°C) inbound (night) pass in Claudette from 2326:00 to 2334:00. Lightning flashes were observed at about 2328:00–2329:00, 2330:00, 2331:00, and 2332:15. (a) Vertical and horizontal electric field (kV m^{-1}); (b) vertical wind speed (m s^{-1}); (c) vertical and horizontal aircraft potential (kV m^{-1}); (d) temperature (°C) and horizontal wind speed (m s^{-1}). No 2D particle image data are available for this pass. (Radar) Single-sweep PPI reflectivity display from the WP-3D lower fuselage radar. The start and end points of the pass are as shown by the long arrow. The aircraft position at the time of the radar image is marked.

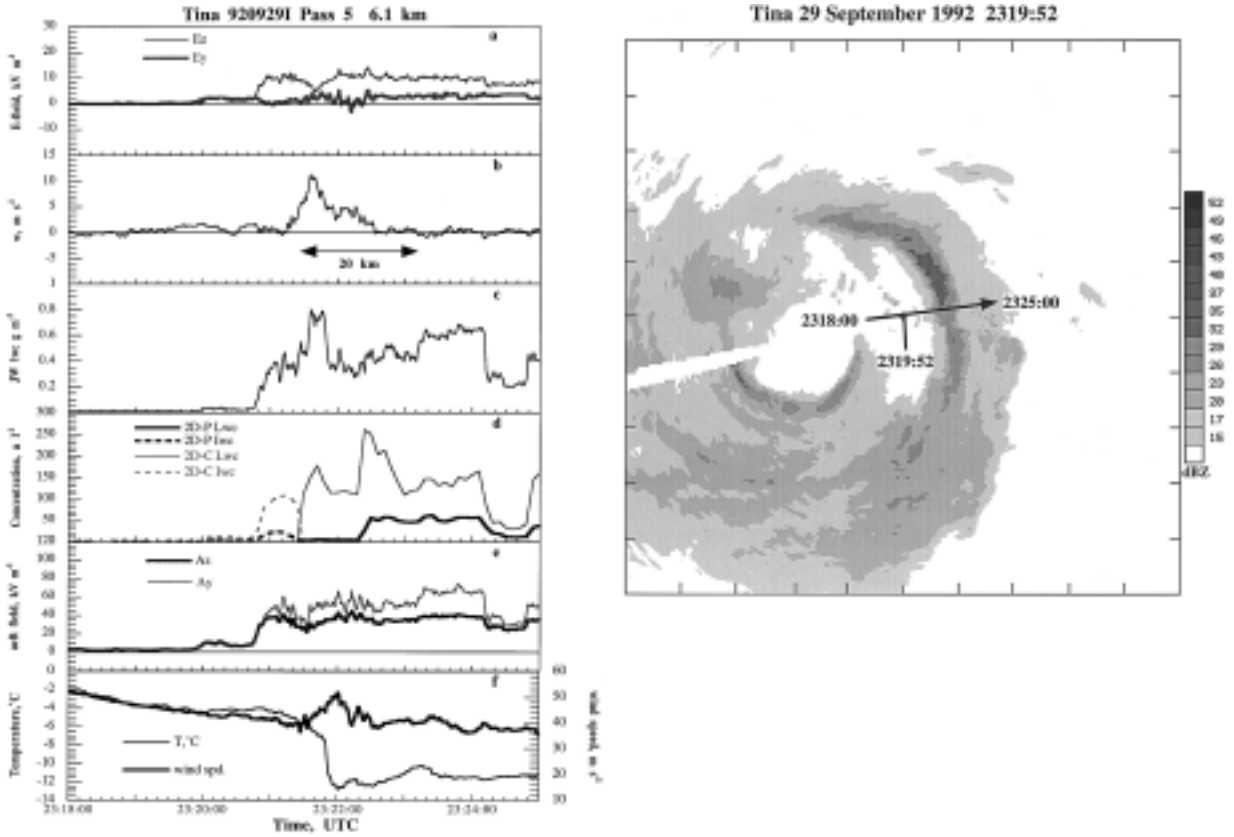

FIG. 13. As in Fig. 5 but for the 6.1-km (−12°C) pass in Tina from 2318:00 to 2325:00. (a) Vertical (E_z) and horizontal (E_y) **E** components (kV m^{-1}); (b) vertical velocity (m s^{-1}); (c) cloud liquid water content from the JW probe (g m^{-3}); (d) particle number concentration (L^{-1}) deduced from 2D particle image data. The 2D-P particle image number concentrations are not scaled. (e) Vertical and horizontal aircraft field (kV m^{-1}) from both pairs of field mills; (f) temperature and horizontal wind speed. (Radar) Single-sweep PPI reflectivity display from the WP-3D lower fuselage radar. The start and end points of the pass are as shown by the long arrow. The aircraft position at the time of the radar image is marked.

out the pass E_y was uniformly weakly positive, with minor exceptions in the updraft at 2331:40 and 2333:00, and in the eyewall remnant at 2237:20. The behavior of E_y in the eyewall remnant from 2336:40 to 2337:00 is consistent with the aircraft having penetrated a node in this component of the field at this spot. The negative excursion occurred just as the larger ice particles disappeared from the image data and the aircraft exited the weak downdraft.

6. Summary

Claudette was much more active electrically than Tina. Claudette exhibited an elevated (50+ dBZ) reflectivity maximum at or slightly above the melting level and ~40-dBZ reflectivity at the −10°C level characteristic of the lightning-producing tropical continental clouds near Darwin, Australia (Zipser and Lutz 1994), plus vertical velocities near the threshold values presented in that paper. Tina was much less impressive in all these respects. Several lightning strikes on the WP-3D were noted by the flight crew before the times of the penetrations given here. The strong convective cell in the northwest eyewall of Claudette had substantial electrical activity, with E_z 25%–50% stronger than in Tina. Further, after the damaging first few encounters with the strong convection in Claudette's eyewall, the aircrew (wisely) refrained from penetrating the most reflective area. Even so, the updrafts observed were usually stronger and wider than those from Tina. Most of Claudette's updrafts contained very large 4−8-mm graupel. No 2D particle image or cloud liquid water data are available for those early passes. In the passes presented here, we have shown that at the lower, warmer temperatures from the melting level to the −5°C level, it is the graupel associated with relatively large positive peaks in E_z. Negative E_z peaks only occurred near the melting level and only when small ice particles were encountered. Within E_z maxima E_y often changed polarity, suggesting that kilometer-sized charge regions advect tangentially about the eye. These observations showed that in all passes, the aircraft passed either into or very near the center of a negatively charged area. Of course, when the updraft exceeds about 10 m s^{-1}, ev-

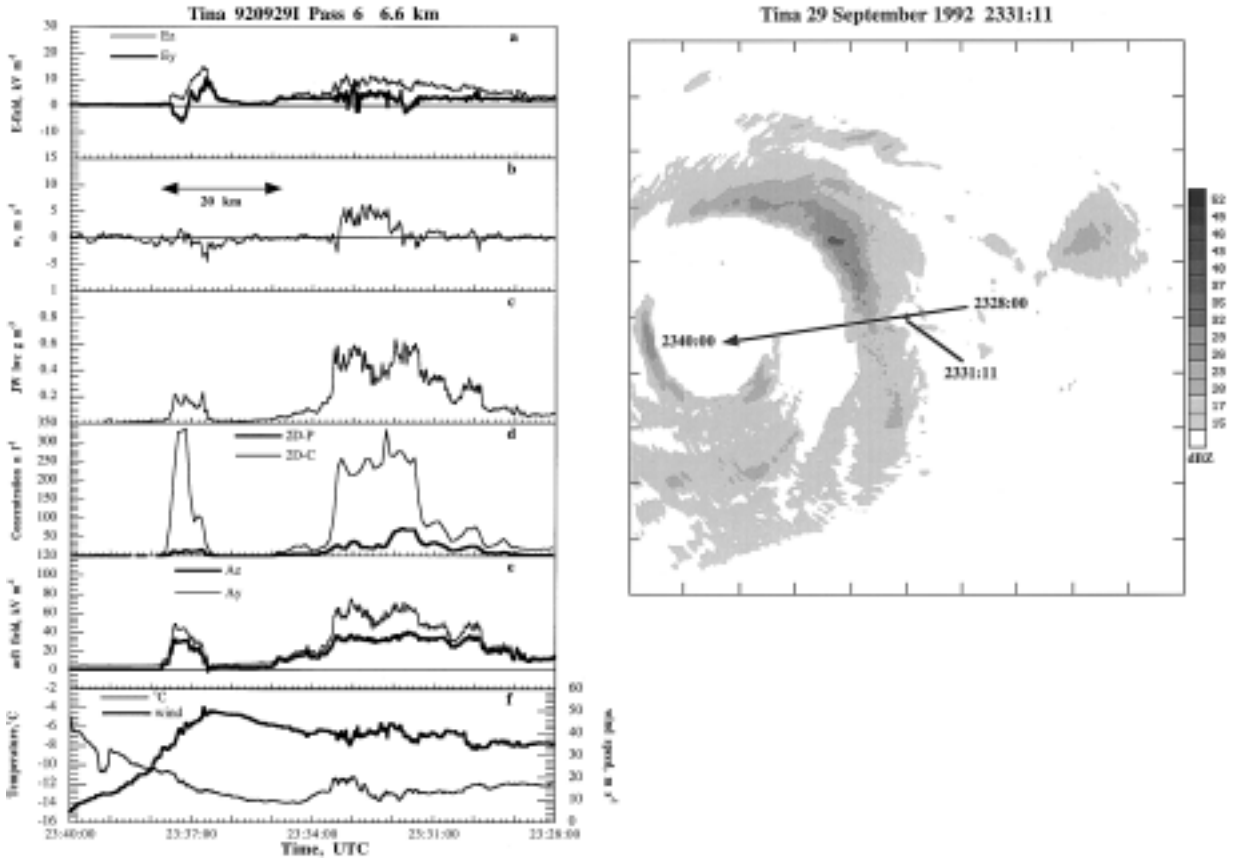

FIG. 14. As in Fig. 5 but for the 6.6-km (−13°C) pass in Tina from 2328:00 to 2340:00. (a) Vertical (E_z) and horizontal (E_y) **E** components (kV m^{-1}); (b) vertical velocity (m s^{-1}); (c) cloud liquid water content from the JW probe (g m^{-3}); (d) particle number concentration (L^{-1}) deduced from 2D particle image data. The 2D-P particle image number concentrations are not scaled. (e) Vertical and horizontal aircraft field (kV m^{-1}) from both pairs of field mills; (f) temperature and horizontal wind speed. (Radar) Single-sweep PPI reflectivity display from the WP-3D lower fuselage radar. The start and end points of the pass are as shown by the long arrow. The aircraft position at the time of the radar image is marked.

erything, including any charge centers or dipoles, is carried to higher altitudes.

In Tina, the updrafts were weak, except for one pass, little or no 4−8-mm graupel was observed, the peak radar reflectivities were near the surface, and the JW showed evidence of erroneous saturation at ~0.8 g m^{-3} of liquid water. These data show that the strongest vertical electric fields were correlated with the presence of ice particles at low altitudes but were not correlated with anything at high altitudes where most particles were ice. The vertical field component sometimes reversed polarity, (suggesting positive over negative) when vapor-grown crystals were numerous, no graupel particles were present, and the temperature was warmer than −5°C. At colder temperatures, E_z was always positive (negative over positive). In Claudette, the strongest fields at low levels were most strongly associated with the 2D-P number concentration, rather than vertical velocity. Above the melting level, the E_z excursions were correlated more with the presence of large graupel and vertical velocity >5 m s^{-1}.

At and above the −10°C level in both storms, both graupel particles in the stronger updraft and all ice particles in the weaker updrafts exist in a positive field. These data are consistent with the idea that both the updrafts and downdrafts at temperatures >−10°C contain an excess of negatively charged particles near the aircraft. The few cases where negative fields predominated were all located in or near downdrafts. From all passes, particularly those in Claudette, E_y was never zero when E_z was nonzero. This showed that the strongest negative charges were offset slightly in the direction of the strongest reflectivity core near the flight track, at or above the −5°C (6.4 km) flight level.

7. Simple model of cloud electrification applied to the hurricane

As we discussed in the introduction, it is necessary to examine several criteria to apply ideas of charge generation and separation in different situations. We begin with the basic assumption that charge separation occurs

by ice interaction processes, which are listed in probable order of importance:

- growing graupel–small ice particle bounce (Takahashi 1978; Saunders et al. 1991);
- particle breakup during melting (Dong et al. 1994); and
- particle evaporation and breakup (Dong and Hallett 1992).

Associated with each process are questions of particle sizes and the amount of charge transferred for each interaction, which is dependent on temperature, LWC, impact velocity, and possibly other parameters. We assume that the separated charge resides on the cloud and precipitation particles and consider the following points:

- the segregation of the separated charge by polarity following differential particle fall velocity;
- advection of charged ice from elsewhere and its interactions with regions of supercooled liquid water;
- the local ice crystal economy—primary nucleation and secondary ice production.

These processes raise fundamental questions in the relation between graupel, small ice, and supercooled water between regions consisting of all supercooled water in the updraft region toward the eye, and completely glaciated downdraft region away from the eyewall.

It is instructive at this point to compare what might be expected in an isolated convective cloud such as might occur in an airmass thunderstorm (or even on an irregular sea-breeze front) and what might be expected in a mature hurricane. The prime difference is the way in which ice produced in prior convection is incorporated into new convection consisting solely of supercooled water. Depending on aerosol origins, primary ice nucleation takes place from $-10°$ to $-20°$C, whereas secondary ice nucleation by rime splintering is active at ambient temperatures from $-4°$ to $-8°$C, or a few degrees colder at high liquid water content (Foster and Hallett 1982; Heymsfield and Mossop 1984). Production of new ice particles by melting or evaporation also occurs wherever the right conditions exist (Oraltay and Hallet 1989). If the cloud reaches only just above the melting level, ice and electrification are both rare (Dye et al. 1986). Qualitatively, supercooled cloud and precipitation (>1-mm drops) can exist at low temperatures ($<-20°$C) as in isolated overland Florida cumuli (Hallett et al. 1978). In this case, the only source of ice is primary nucleation followed by secondary ice production. The case where new convection is seeded from an overlying anvil is common in the hurricane (as in a quasi-symmetrical eyewall or outside the eyewall under the eyewall outflow). In this case, ice particles precipitating from the anvil or circulating in the eyewall effectively nucleate the incipient supercooled cloud before it reaches the $-5°$C level. Hurricane Tina was an example of a storm with a closed eyewall. It follows that charge separation by the graupel–ice process, requiring a temperature from $-5°$ to $-20°$C, will be most likely in storms with strong vertical winds such as Hurricane Emily (1987) and in hurricanes with an asymmetric eye and a developing supercell such as Claudette.

The extensive initiation of ice at warmer temperatures ($>-5°$C) by advection of ice from elsewhere in the hurricane and/or secondary ice production inhibits graupel formation, thereby excluding that process from subsequent electrification. Further, the absence of rapid latent heat release at temperatures between $-5°$ and $-15°$C (as in storms over Florida) may preclude the development of strong vertical velocities (Sax et al. 1979) and further limit the available supercooled water at these levels. Thus the separation of electric charge depends critically on the relative mix of particles on an interface between the updraft (all supercooled water) and downdraft (all ice). This mix varies in the horizontal direction of the vertical shear, or the radial direction from the eye for the hurricane. This horizontal variability evidently varies with temperature at different levels. Charges reverse sign at a given level because of both LWC and temperature changes and are depicted schematically in Fig. 15, following Saunders et al. (1991) and Willis et al. (1994). Observation of the details of the microphysical processes requires high spatial resolution measurements of ice and cloud water particles, necessitating the use of instruments such as the FORMVAR replicator. We recognize that the presence of graupel, cloud droplets, and small ice crystals in the same air parcel such that they can be inferred to be interacting is difficult to measure. It is possible to draw false conclusions when combining measurements from two (necessarily) noncollocated probes, which do not sample the same air parcel.

Interpretation of these data is complicated by the fact that the eyewall updraft, and the area suitable for charge separation, tilts radially outward on average about 45°–50°. In addition, particles are rapidly advected tangentially away from the updrafts. Under such circumstances, if, as we believe, larger ice particles acquire one charge, and small ones the opposite, then the charge center dominated by the larger particles cannot be directly below that dominated by the smaller ice particles, and the dipole is tilted outward (see Fig. 16). Similarly, the strong wind shear in the eyewall acts to spread the charged particles over a large area, thereby weakening both the horizontal and vertical gradients of charge. This effect alone would result in a smaller number of lightning strokes per coulomb of separated charge in a hurricane and may explain the preponderance of positive field in these measurements. Of course, the polarity of the fields may also be simply a function of the flight altitude.

The occurrence of an electrical discharge (lightning flash) requires a separation of about 10 C of charge per flash (a typical negative CG lightning discharge consists of several strokes and lowers tens of coulombs to ground; Uman 1987). Charge densities in a hurricane

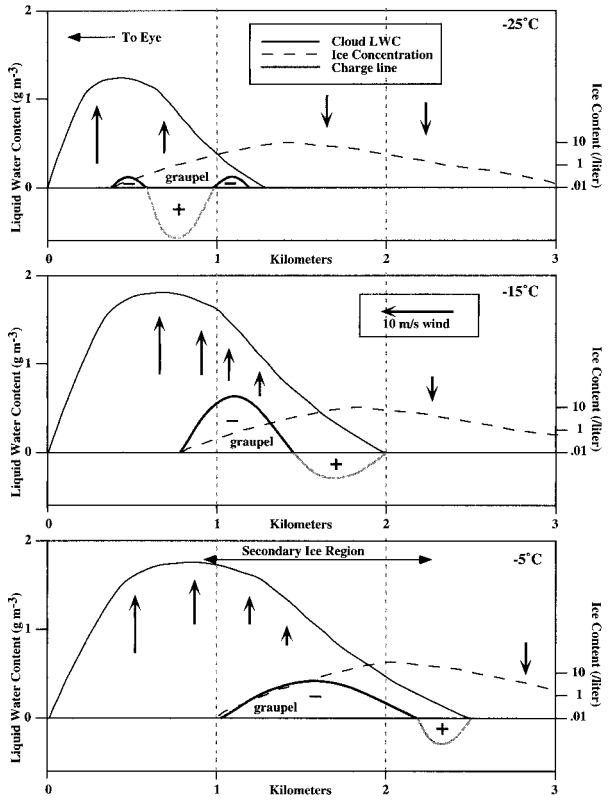

FIG. 15. Idealized cross section through the upshear side of an updraft containing supercooled liquid water and a downshear ice-containing downdraft as might occur in a hurricane eyewall (with circular symmetry) or locally in a deep convective cloud. The charge separation protocol was taken from Saunders et al. (1991; Fig. 7); other scenarios are possible. Arrows indicate local vertical velocity, and the expected location of graupel particles is shown. Separation of charge resulting from ice–graupel collisions depends on the relative concentration of particles and the magnitude of the liquid water content; the sign and magnitude of the charge on the target (larger) particle is indicated, as inferred from laboratory data. The sign and magnitude of the separated charge varies with location both along the horizontal (as measured by aircraft penetrations perpendicular to the horizontal wind) and in the vertical (from aircraft penetrations at different temperatures). The relative concentration of vapor-grown ice results from splinter production by the Hallett–Mossop process under appropriate conditions. Subsequent vertical and downshear advection of the particles determines the LWC to ice transition. The charging processes are controlled by the rate at which splinters are captured by supercooled drops to form new rimers and produce yet more splinters under appropriate conditions and the rate of bounce of such particles from growing graupel.

are not known, and postulating the existence of a simple spherical or flat layered charge structure is clearly inadequate. Assuming a charge density of ~5 C km^{-3} (Winn et al. 1981), this implies charged volumes of at least 2–4 km^3 per flash, to be replenished by active processes to maintain a given flash rate. The mere existence of measurable electric field does not necessarily imply the occurrence of any lightning discharge, as is clearly the case for the symmetrical eyewall.

To estimate the rate at which a hurricane eyewall can separate charge, we first recognize that active [the strongest 10% of the draft cores, as defined by Jorgensen et al. (1985)] convective updrafts occupy about half of the convective area in the eyewall, as shown by numerous aircraft penetrations (Black and Hallett 1986; Black et al. 1994; and others). Note that we do not refer to the areal extent of high radar reflectivity, since supercooled cloud liquid water is not detectable by radar. (We note that supercooled raindrops can be remotely detected by polarization diversity radar, if available.) Further, these updrafts are generally about 4 km in diameter (Jorgensen et al. 1985) in the typical hurricane and up to 7 km in the extreme case of Hurricane Emily (Black et al. 1994). In Claudette above the melting level, the corresponding figure is 6 km wide. We know from direct observation in Claudette and Tina that the updrafts extend from 5.0- to at least 7.0-km altitude, and there is less than 0.5 g m^{-3} of cloud LWC (in Tina) at or above 7.0 km. If we assume that the region of charge separation corresponds to the updraft area and that the eye diameter is 40 km (a typical value for an electrified hurricane such as Claudette), we have about 800 km^3 in which we can separate charge. This volume is reduced further to about 200 km^3 if we assume that only 25% of this volume contains active updraft, as in an asymmetric storm like Claudette.

As shown in Fig. 15, the region of charge separation is somewhat less than the updraft width and is more likely to extend over a kilometer or less where the mix of particles is optimum. The conceptual model is of an upshear updraft containing supercooled water, evolving (in a radial sense) on the eye side and being eroded outward from the eye by lateral diffusion of ice from the downdraft. Thus the region of optimum mix is in a quasi-steady state and results in a net charge distribution following gravitational separation and the geometry of the spatial redistribution in the vertical and horizontal motion. The greatest radar signal, dominated by the maximum of ND^6 (N, concentration; D, diameter), will signal where the graupel particles are large and numerous, a few kilometers *downshear* of these regions, not necessarily where supercooled water is present. Thus charge separation regions will compose a highly convoluted three-dimensional surface, almost continuous in a linear system (as in a sea-breeze front or symmetrical eyewall), but discontinuous and wrapped around in the direction of the shear in an individual convective cell.

Our working hypothesis is that ice particle collisions in the presence of cloud liquid water are necessary to separate charge. If we assume that each collision of a graupel particle with a smaller ice particle in a hurricane separates an average of 10×10^{-15} C (on the low side of the experimental results of Saunders et al. 1991), we can estimate the number of collisions (1×10^{15}) necessary to separate the required 10 C of charge. If the actual average charge separated per collision is larger, the number of collisions required is reduced proportionally. The fall speed of a 4-mm graupel particle at the 500-mb level is about 2 m s^{-1}. Assume that the

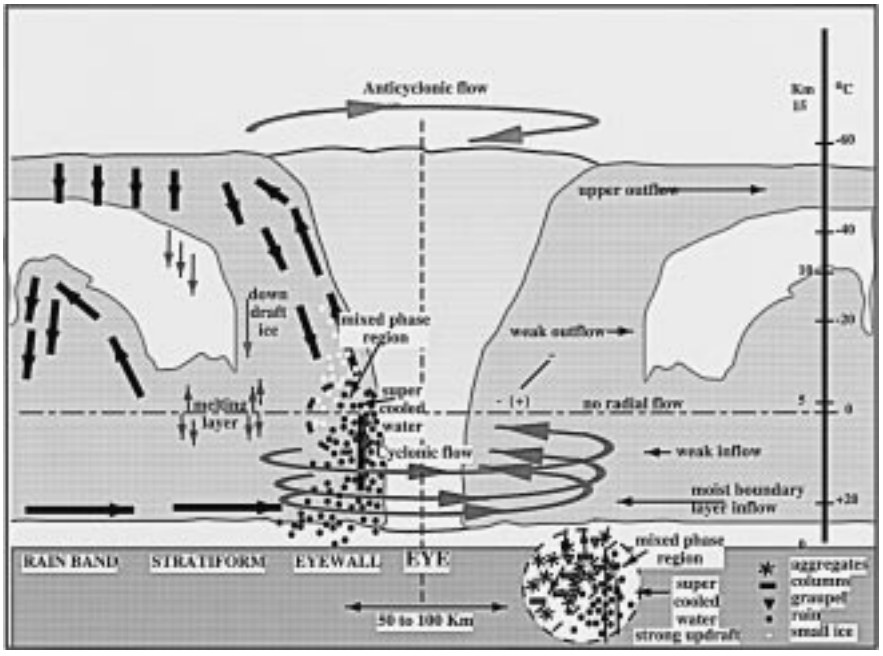

FIG. 16. Schematic depicting hurricane precipitation processes, cloud distribution, and preferred regions for charge separation. Ocean surface temperatures are near 28°C giving cloud-base temperatures near 22°C. In mature hurricanes, typical vertical velocities near 0°C level are 5–8 m s^{-1}, with convection extending to well beyond the −40°C isotherm, the temperature for homogeneous ice nucleation. The inset shows the region where charge separation occurs in the horizontal gradient of vertical shear, limited in altitude by the lack of supercooled water above −5°C. White dots indicate where small ice particles, frozen drops, and graupel exist, and black drops indicate rain. Air motion arrows show axial and radial flow leading to redistribution of hydrometeors. Tangential (primary) circulations are represented by fat arrows with elliptical tails; note the change from cyclonically curved flow to anticyclonic outflow near the top of the storm and ice redistribution at midlevels. Thinner, straight arrows show approximate radial and vertical air motions; lengths are not to scale. The observed distribution of electric field polarity is shown.

average updraft is 6 m s^{-1}, so that the 4-mm graupel requires about 500 s to traverse the mixed-phase area. A hurricane updraft in the ice region (e.g., Figs. 9, 11, 13) typically contains about 80–50 ice particles per liter, of which about 4–10 are millimeter (and larger) graupel. At a relative speed of about 1 m s^{-1}, one such graupel particle would make about 5000 collisions (10 s^{-1}) in the mixed-phase region, thus 2×10^{11} large graupel particles are needed to produce one lightning flash every 500 s, and at four large graupel particles per liter (L), 5×10^{11} L (50 km^{-3}) of mixed-phase region are needed. With only about 217 km^{-3} available, this hypothetical hurricane could produce about four lightning flashes every 500 s, or 750 flashes per day. Compare this to the ~10 h^{-1} (240 per day) flash rate in Andrew's eyewall prior to its landfall in southern Florida (Molinari et al. 1994, plate 2B), a time that included a rapid deepening event (Holliday and Thompson 1979). Merely halving one of the three major variables (average charge separated per collision, the concentration of graupel, or the volume of the mixed-phase region) equals the Andrew flash rate. Claudette (during the flight considered here) was probably producing at least as much CG lightning as Andrew, and it certainly had more than 4 L^{-1} of large graupel in its eyewall updrafts. Hurricanes undergoing rapid deepening are known to have stronger vertical motions than usual (Black et al. 1994), with the ability to change the microphysics and produce lightning. Numerical modeling of such a system clearly presents a major challenge and depends critically on the assumptions made of the structure of the ice–supercooled cloud interface and the details of the charge separation processes indicated in Fig. 15. Clearly, additional measurements of the microphysical properties of such regions are needed, to be related to the overall hurricane structure as shown in Fig. 16. We need to make microphysical and electrical measurements at higher, colder levels than can be reached with the WP-3D.

8. Conclusions

Our studies suggest that distinct microphysical conditions govern the magnitude and sign of the charge separation process. We interpret the prevalence of net negative charge at temperatures above −13°C with the aid of Fig. 15 (derived from laboratory results discussed

in section 2) as a variation of the charge separation *along* the shear. In a deep cloud with supercooled water extending to temperatures as low as −20°C, a positive polarity dipole (positive above negative) results, together with a dipole of opposite polarity lower down. In our case, a negative polarity dipole (negative above positive) *at temperatures above −13°C is all we see.* The polarity of **E** depends on the relative concentrations of particles in the cloud and which dipole dominates. Thus the macroscopic mixing process and the cloud droplet size distribution at the up/down vertical velocity interface is controlling the charge separation. Our results in the hurricane eyewall suggest that the negative above positive dipole dominates. This suggests in turn that the secondary ice crystal production rate is critical, as it dominates the reduction in LWC in these regions.

Little evidence for net negative E_z was observed at any location at any level in any hurricane, except in weak downdrafts near the melting level. Net positive vertical electric fields everywhere argue against the accumulation of large quantities of positively charged particles at temperatures warmer than −13°C in the hurricane. Further, if many positively charged particles existed at higher altitudes, few of them are advected to the flight-level altitudes. Only at temperatures warmer than −5°C were predominantly positive polarity (positive over negative) fields encountered in a few locations, and these were exclusively where very small (apparently vapor grown) columns and needles were the only ice particles present. This lends credence to the idea that the majority of the larger particles acquire negative charge, leading to the observed negative polarity (negative over positive dipole) and the submillimeter-sized vapor-grown crystals, positive at all locations up to 7-km altitude. Our (limited) LWC data indicates that in the hurricane updraft at temperatures <-5°C, peak LWC is $\leq\sim 1$ g m^{-3}, and LWC is <0.2 g m^{-3} elsewhere. These observations of predominantly net negative **E** in areas containing particles $>\sim 1$ mm in diameter are consistent with the laboratory experiments of Takahashi (1978) for cloud LWC >1 g m^{-3} and temperature <-10°C, and those of Saunders et al. (1991) for LWC >0.2 g m^{-3} and temperatures >-15°C. As peak LWC is almost always less than 1 g m^{-3} in the −10° to −15°C range, this suggests that neither the Takahashi (1978) nor the Saunders et al. (1991) results fully explain these observations. The solution to this problem may lie with the cloud droplet size distributions, which Saunders and Peck (1998) pointed out have a substantial impact upon the particle charging. We acknowledge that high local ice supersaturation may be produced in regions just above the melting level should partly melted ice particles become incorporated into an updraft and advect into regions below 0°C. Under such circumstances, elastic collisions could occur among rapidly growing ice particles leading to considerable charge separation. This effect needs further study, as there is conventional wisdom that more aircraft lightning strikes occur near the melting level than elsewhere (Fisher and Plummer 1977).

It is likely that, in the updraft in regions with moderate ice content near the interface with the downdraft, low LWC (~ 0.2 g m^{-3}) still occurs, which (according to Saunders et al. 1991) can lead to positive rimer charge and an inverted dipole. It is unlikely that LWC is low everywhere, especially in the upshear edge of the eyewall in the strong updrafts of Claudette (although this is possible in parts of Tina). Thus, we seek an explanation in terms of the idea that most of the charge separation in the eyewall occurs in modest LWC regions. This implies that a sharp transition occurs from areas with some graupel, little small ice, and much water to areas with some graupel, lots of small ice, and little cloud water. These observations also fail to support the hypothesis of Williams et al. (1994) for positive charging during deposition growth in stratiform clouds, in that the hurricane stratiform areas are either weakly charged or uncharged. This is shown by both direct electric field measurements (e.g., Figs. 13 and 14) and by remote lightning detection, which shows that the vast majority of detected CG lightning in the hurricane occurs in or near convective areas (Molinari et al. 1994; Samsury and Orville 1994). In comparison with our data, balloon-borne electric field measurements obtained in MCS systems and convection over the Great Plains (Marshall et al. 1995) show **E** that is up to five times stronger than in the hurricane and has two or more polarity changes in the zone from the melting level to about −10°C. Of course, storms like those sampled by Marshall et al. (1995) also typically produce much more CG lightning per unit time than hurricanes do. The strong horizontal and vertical advection of particles in a hurricane could easily disrupt any multiple-layered charge structures.

Simultaneous cloud water content and particle charge measurements are an important omission in these data. Earlier hurricane studies (e.g., Black and Hallett 1986) have shown that 6–10-m s^{-1} updrafts such as were observed here typically contain $0.25 <$ LWC < 2 g m^{-3} of cloud liquid water at the −5°C level. Such updrafts can lift 5–6-mm diameter raindrops. Claudette's eyewall updrafts often contained several grams per cubic meter of supercooled rain at $T > -5$°C, so it is reasonable to assume that cloud water contents were also substantial. Clearly, better cloud LWC data in cold conditions are needed to resolve this problem. The question initially posed still remains: how much initial precipitation formed by coalescence falls out and how much is lofted to lower temperatures and passes through the ice phase prior to falling out?

Nevertheless, the existence of substantial electric fields in Claudette and Tina shows that charge separation was occurring in those storms. Further, the numerous lightning flashes observed from the aircraft in Claudette show that the charge separation was occurring swiftly enough to produce lightning. Crude calculations of the

expected flash rate in Claudette yielded a flash rate of about 30 h^{-1}, compared to the 10 h^{-1} CG flash rate observed in Hurricane Andrew, a rate that is known to underestimate the total flash rate (including intracloud flashes). The most significant difference between these storms was the existence of copious large graupel in the Claudette updrafts, similar to that observed in Hurricane Emily.

The measurement of electric field in precipitating clouds is one of the more challenging observations in atmospheric science. In the hurricane, charge separation can occur in multiple locations simultaneously in a complex particle mix, and the strong horizontal winds ensure that charged particles become widely dispersed in a relatively short time. As coincident satellite-based observations of lightning and airborne ice particle (morphology and charge) measurements in hurricanes at higher altitudes become available, the relationships between the microphysics—the amount of precipitation originating as ice and water, the electrification in the ice containing regions, and the storm dynamics—will become clearer.

Acknowledgments. We express our appreciation to the AOC personnel for assisting with instrumentation and flight operation on the NOAA WP-3D aircraft. We are indebted to Rick Purcell of DRI, who was indispensable in the design and construction of the instrumentation for electrical measurements on the WP-3D. J. Hallett was supported by National Science Foundation Grants ATM 9021918 and ATM 9113908, and a grant with NOAA, Contract 50-WCNR-1-06054 for participation in the flight program.

APPENDIX

Calibration of the Airborne Field Mill System

Calibration of an airborne field mill system is difficult. Unlike some aircraft used for meteorological research, the WP-3D exhibits a self-charge in clear-air flight that precludes measurement fields smaller than $\sim$1.5 kV m^{-1} (i.e., some 15 times fair weather values). The magnitude of the self-charge varied slightly with a number of variables including altitude, air speed, and engine setting characteristics. The reason for this self-charge is not clear; WP-3D engines exhaust over the wing, passing over $\sim$0.7 m of soot covered aluminum sheet metal. We conjecture that soot particles/ions are collected during this passage to give the aircraft a net charge. Soot particles typically carry net negative charge (a few electrons per particle; Mayo and Weinberg 1970), so if particles are collected, the aircraft becomes negatively charged. During flights through rain in Hawaii at cloud temperatures entirely above 0°C (so-called warm rain) the National Center for Atmospheric Research Electra aircraft (a civilian version of the WP-3D) becomes charged equivalent to $\sim$15 fine weather fields (1.5 kV m^{-1}), which gives a measure of the lower limit of detection of ambient field. Thunderstorm fields are $\sim$50 times this value (some 10 times less than breakdown voltage at 1000 hPa, about 1000 kV m^{-1}).

Other complicating factors arise because the aluminum aircraft skin is painted with nonconducting paint, thereby allowing unbalanced local charges to accumulate. Further, the lower fuselage radome can also acquire static charge. Asymmetric static charges on the aircraft skin produced by ice particle impacts can render electric field measurements in clouds unreliable (Harris-Hobbs et al. 1994). We gauge the effects of charge on the aircraft by monitoring **E** components produced by such charge. The electric field caused by aircraft charge is computed as the sum of the output from each pair of mills divided by two. These quantities (A_z and A_y) compose independent estimates of the effects of charge on the aircraft. In this work, we argue that the estimate of **E** is good if the A_z and A_y estimates vary in phase with each other, because unbalanced static charges on the aircraft skin would cause these two independent measurements to diverge.

Each mill is given an absolute calibration in the laboratory using horizontal plates charged at +1.0, +5.0, and +25.0 kV m^{-1}. Mills mounted on the aircraft are calibrated as required with a portable plate charged to $\pm$2.3 kV and placed at a fixed distance from each mill. While none of this is sufficient to provide the ambient electric field in flight, this procedure does ensure that the mills measure the local electric field and give the correct polarity. The vertical upward mill is mounted on a pylon extending approximately 30 cm above the aircraft skin. The vertical down mill is mounted on a flat plate 60 cm in diameter, and the side mills are mounted looking horizontally. For structural reasons, these mills are offset slightly from their nominal orientation and location (Fig. 1). The field mills are not flush with the aircraft skin; each mill projects 1.5 cm from the skin to prevent water flowing along the skin from flooding the mills. Some data from the upper mill were lost because of rainwater leakage that occurred during heavy precipitation while the aircraft was parked. Also, some data from the upper mill are suspect because the support pylon was painted and thus subject to local accumulation of static charge from ice particle impacts.

In order to measure ambient electric fields from an aircraft, field mill outputs must also be reduced by a factor to account for the enhancement of the local fields caused by the convergence of electric field lines onto the curved metal aircraft skin. Determining the absolute enhancement coefficients is not a trivial task for a large aircraft like the WP-3D. Direct methods, such as lifting the (charged) aircraft with an insulated crane high enough to avoid producing induced ''image'' charges on the ground, are impractical. The WP-3D is also too large to make turns at $>\sim30°$ of roll, and finding a more or less uniformly charged anvil big enough to make such wide turns is extremely difficult. Charge-transfer meth-

TABLE A1. Field mill enhancement coefficients used on these data.

Upper	Lower	Right	Left
6.1	3.2	2.6	2.0

ods (such as that used by Harris-Hobbs et al. 1994) that make use of a conducting scale model of the aircraft could be carried out with considerable effort.

The relative enhancement coefficients were determined during flights in electrically undisturbed clear air from the response of the mills to the aircraft self-charge in combination with a high-voltage supply (18 kV). The aircraft was subjected to a controlled self-charge in a sense opposite to the engine effect by discharge through a series of insulated needle points mounted below the aircraft. The voltage and current (+1 ma) were measured during flight. Since the response of the mills to the power supply mimicked the responses from the aircraft self-charge, we used the self-charge to determine the relative enhancement factors. With the aircraft fully self-charged, the mill that responded least was assigned the basic enhancement value of 2.0 (appropriate for mills mounted on an infinite conducting cylinder), and the others were increased in proportion to their response (Table A1). Differences in the mill enhancement factors occur because the aircraft is not an infinite cylinder; hence, these factors change with mounting location. Similar variations in the enhancement factors were present in the matrix analysis of Kositsky et al. (1991) using enhancement factors derived from a conducting model. Other researchers (e.g., Mazur et al. 1987; Harris-Hobbs et al. 1994), using flush-mounted mills on smaller aircraft, have reported enhancement values in the range of 1.2–2.2 for the field component normal to the mill for mills located in similar places near the midpoint of the fuselage. We have ignored cross-terms in the transformation, which we assess limits our uncertainty to some ±10% under adverse circumstances. Based upon the results of Harris-Hobbs et al. (1994), we expect that the enhancement coefficients that we determined for these fuselage-mounted mills are within a 20% uncertainty. The mill responses were plotted for clear weather conditions at altitudes from 0.5 to 6.0 km, and the average response over these altitudes was used. No mill output varied by more than 5% over the entire range of altitudes in these conditions.

After application of these corrections to the raw mill output values, the calibrated electric field components are derived in the following way. $E_z = (E_{\text{down}} - E_{\text{up}})/2.0$, such that positive E_z occurs when any of the following conditions exists: E_{down} and E_{up} are both larger than zero, with $E_{\text{down}} > E_{\text{up}}$; E_{down} and E_{up} are both less than zero, with $|E_{\text{up}}| > |E_{\text{down}}|$; or $E_{\text{down}} > 0$, $E_{\text{up}} < 0$, and $|E_{\text{down}}| > |E_{\text{up}}|$. Therefore, a negative charge center located above the aircraft is indistinguishable from a positive charge center below the aircraft, and vice versa. The E_y component is computed in a similar manner, with $E_y = (E_{\text{right}} - E_{\text{left}})/2.0$, and ambiguities similar to those for E_z apply to E_y. In the data from this study, however, since precipitation static caused a buildup of negative charge on the aircraft, all mills generally recorded positive values.

REFERENCES

Anthes, R. A., 1982: *Tropical Cyclones: Their Evolution, Structure and Effects.* Amer. Meteor. Soc., 208 pp.

Baumgardner, D., 1983: Analysis and comparison of five water droplet measuring devices. *J. Climate Appl. Meteor.,* **22,** 891–910.

——, W. Strapp, and J. E. Dye, 1985: Evaluation of the Forward Scattering Spectrometer Probe. Part II: Corrections for coincidence and dead-time losses. *J. Atmos. Oceanic Technol.,* **2,** 626–632.

Black, M. L., R. W. Burpee, and F. D. Marks Jr., 1996: Vertical motion characteristics of tropical cyclones determined with airborne Doppler radial velocities. *J. Atmos. Sci.,* **53,** 1887–1909.

Black, P. G., R. A. Black, J. Hallett, and W. A. Lyons, 1986: Electrical activity of the hurricane. Preprints, *Conf. on Cloud Physics,* Snowmass, CO, Amer. Meteor. Soc., J277–J280.

Black, R. A., 1990: Radar reflectivity–ice water content relationships for use above the melting level in hurricanes. *J. Appl. Meteor.,* **29,** 955–961.

——, and J. Hallett, 1986: Observations of the distribution of ice in hurricanes. *J. Atmos. Sci.,* **43,** 802–822.

——, H. B. Bluestein, and M. L. Black, 1994: Unusually strong vertical motions in a Caribbean hurricane. *Mon. Wea. Rev.,* **122,** 2722–2739.

Brook, M., P. Krehbiel, D. MacLaughlan, T. Takeuti, and M. Nakano, 1980: Positive ground stroke observations in Japanese and Florida storms. *Proceedings in Atmospheric Electricity,* L. H. Ruhnke and J. Latham, Eds., A. Deepak, 365–373.

Brooks, I. M., C. P. R. Saunders, R. P. Mitzeva, and S. L. Peck, 1997: The effect on thunderstorm charging of the rate of rime accretion by graupel. *Atmos. Res.,* **43,** 277–295.

Case, B., and M. Mayfield, 1990: Atlantic hurricane season of 1989. *Mon. Wea. Rev.,* **118,** 1165–1177.

Cerni, T. A., 1983: Determination of the size and concentration of cloud drops with an FSSP. *J. Climate Appl. Meteor.,* **22,** 1346–1355.

Cooper, W. A., 1988: Effects of coincidence on measurements with a Forward Scattering Spectrometer Probe. *J. Atmos. Oceanic Technol.,* **5,** 823–832.

Dong, Y. Y., and J. Hallett, 1992: Charge separation by ice and water drops during growth and evaporation. *J. Geophys. Res.,* **97,** 20 361–20 371.

——, R. G. Orltay, and J. Hallett, 1994: Ice particle generation during evaporation. *Atmos. Res.,* **32,** 45–53.

Dye, J. E., and Coauthors, 1986: Early electrification and precipitation development in a small, isolated Montana cumulonimbus. *J. Geophys. Res.,* **91,** 1231–1247.

Fisher, F. A., and J. A. Plummer, 1977: Lightning protection of aircraft. NASA Rep. NASA-RP-1008, 550 pp. [NTIS N78-11024/4/XAB.]

Foster, T., and J. Hallett, 1982: A laboratory investigation of the influence of liquid water content on the temperature dependence of secondary ice crystal production during soft hail growth. Preprints, *Conf. on Cloud Physics,* Chicago, IL, Amer. Meteor. Soc., 123–126.

Gamache, J. F., F. D. Marks Jr., and F. Roux, 1995: Comparison of three airborne Doppler sampling techniques with airborne in situ wind observations in Hurricane Gustav (1990). *J. Atmos. Oceanic Technol.,* **12,** 171–181.

Gardiner, B. A., and J. Hallett, 1985: Degradation of in-cloud forward

scattering spectrometer probe measurements in the presence of ice particles. *J. Atmos. Oceanic Technol.,* **2,** 171–180.
Hallett, J., and S. C. Mossop, 1974: Production of secondary ice particles during the riming process. *Nature,* **249,** 26–28.
——, R. I. Sax, D. Lamb, and A. S. R. Murty, 1978: Aircraft measurements of ice in Florida cumuli. *Quart. J. Roy. Meteor. Soc.,* **104,** 631–651.
Harris-Hobbs, R., K. L. Giori, M. Bellmore, and A. Lunsford, 1994: Application of airborne field mill data for use in launch support. *J. Atmos. Oceanic Technol.,* **11,** 738–750.
Heymsfield, A. J., and S. C. Mossop, 1984: Temperature dependence of secondary ice particle production during soft hail growth by Riming. *Quart. J. Roy. Meteor. Soc.,* **110,** 765–720.
Holliday, C. R., and A. H. Thompson, 1979: Climatological characteristics of rapidly intensifying typhoons. *Mon. Wea. Rev.,* **107,** 1022–1034.
Hudson, J. G., and P. R. Frisbie, 1991: Cloud condensation nuclei near marine stratus. *J. Geophys. Res.,* **96** (D11), 20 795–20 808.
Jayaratne, E. R., C. P. R. Saunders, and J. Hallett, 1983: Laboratory studies of the charging of soft hail during ice crystal interactions. *Quart. J. Roy. Meteor. Soc.,* **109,** 609–631.
Jones, J. J., W. P. Wynn, and F. Han, 1993: Electric field measurements with an airplane: Problems caused by emitted charge. *J. Geophys. Res.,* **98,** 5235–5244.
Jorgensen, D. P., 1984a: Mesoscale and convective-scale characteristics of mature hurricanes. Part I: General observations by research aircraft. *J. Atmos. Sci.,* **41,** 1268–1285.
——, 1984b: Mesoscale and convective-scale characteristics of mature hurricanes. Part II: Inner core structure of Hurricane Allen (1980). *J. Atmos. Sci.,* **41,** 1287–1311.
——, and M. A LeMone, 1989: Vertical velocity characteristics of oceanic convection. *J. Atmos. Sci.,* **46,** 621–640.
——, E. J. Zipser, and M. A. LeMone, 1985: Vertical motions in intense hurricanes. *J. Atmos. Sci.,* **42,** 839–856.
Kositsky, J., K. L. Giori, R. A. Maffione, D. H. Cronin, J. E. Nanevicz, and R. Harris-Hobbs, 1991: Airborne field mill (ABFM) calibration report, SRI Project 1449, Task A, Final Report, 368 pp. [Available from SRI International, 333 Ravenswood Avenue, Menlo Park, CA 94025-3493.]
LeMone, M. A., and E. J. Zipser, 1980: Cumulonimbus vertical velocity events in GATE. Part I: Kinematic structure. *J. Atmos. Sci.,* **37,** 2444–2457.
Lenschow, D. H., and W. T. Pennel, 1974: On the measurement of in-cloud and wet-bulb temperatures from an aircraft. *Mon. Wea. Rev.,* **102,** 447–454.
Lopez, R. E., R. F. Reinking, J. Hallett, and D. Rosenfeld, 1985: 5-cm radar echoes and their microphysical significance in Florida cumuli. *J. Geophys. Res.,* **90,** 10 667–10 673.
Ludlum, D. M., 1963: *Early American Hurricanes 1492–1870.* Amer. Meteor. Soc., 198 pp.
Lyons, W. A., and C. S. Keen, 1994: Observations of lightning in convective supercells within tropical storms and hurricanes. *Mon. Wea. Rev.,* **122,** 1897–1916.
Marks, F. D., Jr., and R. A. Houze Jr., 1987: Inner core structure of Hurricane Alicia from airborne Doppler radar observations. *J. Atmos. Sci.,* **44,** 1296–1317.
Marshall, T. C., W. D. Rust, and M. Stoltzenberg, 1995: Electrical structure and updraft speeds in thunderstorms over the southern Great Plains. *J. Geophys. Res.,* **100,** 1001–1015.
Mayo, P. J., and F. J. Weinberg, 1970: On the size, charges and number-rate of formation of carbon particles: Influences subject to electric fields. *Proc. Roy. Soc. London,* **319A,** 351–371.
Mazur, V., L. H. Ruhnke, and T. Rudolph, 1987: Effect of E-field mill location on accuracy of electric field measurements with instrumented aircraft. *J. Geophys. Res.,* **92,** 12 013–12 019.
Molinari, J., P. K. Moore, V. P. Idone, R. W. Henderson, and A. B. Saljoughy, 1994: Cloud-to-ground lightning in Hurricane Andrew. *J. Geophys. Res.,* **99,** 16 665–16 676.
Mossop, S. C., 1985: Secondary ice particle production during rime growth: The effect of drop size distribution and rimer velocity. *Quart. J. Roy. Meteor. Soc.,* **111,** 1113–1124.
Oraltay, R. G., and J. Hallett, 1989: Evaporation and melting of ice crystals: A laboratory study. *Atmos. Res.,* **24,** 169–189.
Pasch, R. J., and L. A. Avila, 1992: Atlantic hurricane season of 1991. *Mon. Wea. Rev.,* **120,** 2671–2687.
Reynolds, S. E., M. Brook, and M. F. Gourley, 1957: Thunderstorm charge separation. *J. Meteor.,* **14,** 426–436.
Rust, D., and T. C. Marshall, 1996: On abandoning the thunderstorm tripole-charge paradigm. *J. Geophys. Res.,* **101** (D18), 23 499–23 504.
Rutledge, S. A., E. R. Williams, and T. D. Keenan, 1992: The Down Under Doppler Experiment (DUNDEE): Overview and preliminary results. *Bull. Amer. Meteor. Soc.,* **73,** 3–16.
Samsury, C. E., and R. E. Orville, 1994: Cloud-to-ground lightning in tropical cyclones: A study of Hurricanes Hugo (1989) and Jerry (1989). *Mon. Wea. Rev.,* **122,** 1887–1896.
Saunders, C. P. R., and I. M. Brooks, 1992: The effects of high liquid water content on thunderstorm charging. *J. Geophys. Res.,* **97,** 14 671–14 676.
——, and S. L. Peck, 1998: Laboratory studies of the influence of the rime accretion rate on charge transfer during crystal/graupel collisions. *J. Geophys. Res.,* **103** (D12), 13 949–13 956.
——, W. D. Keith, and R. P. Mitzeva, 1991: The influence of liquid water on thunderstorm charging. *J. Geophys. Res.,* **96,** 11 007–11 017.
Sax, R. I., J. Thomas, M. Bonebrake, and J. Hallett, 1979: Ice evolution within seeded and nonseeded Florida cumuli. *J. Appl. Meteor.,* **18,** 203–214.
Simpson, G., and J. J. Scrase, 1937: The distribution of electricity in thunderclouds. *Proc. Roy. Soc. London,* **161A,** 309–352.
Simpson, R. H., and H. Riehl, 1981: *The Hurricane and Its Impact.* Louisiana State University Press, 397 pp.
Takahashi, T., 1978: Riming electrification as a charge generation mechanism in thunderstorms. *J. Atmos. Sci.,* **35,** 1536–1548.
Uman, M. A., 1987: *The Lightning Discharge.* International Geophysics Series, Vol. 39, Academic Press, 377 pp.
Williams, E. R., 1995: Meteorological aspects of thunderstorms. *Handbook of Atmospheric Electrodynamics,* Hans Volland, Ed., CRC Press, 27–60.
——, R. Zhang, and D. Boccipio, 1994: Microphysical growth state of ice particles and large-scale electrical structure of clouds. *J. Geophys. Res.,* **99,** 10 787–10 792.
Willis, P. T., and J. Hallett, 1991: Microphysical measurements from an aircraft ascending with a growing isolated maritime cumulus tower. *J. Atmos. Sci.,* **48,** 283–300.
——, F. D. Marks Jr., and J. Hallett, 1991: Tracing the interactions of precipitation evolution and cloud dynamics using airborne doppler radar and in-situ data. *Preprints, 25th Int. Conf. on Radar Meteorology,* Paris, France, Amer. Meteor. Soc., 916–919.
——, J. Hallett, R. A. Black, and W. Hendricks, 1994: An aircraft study of rapid precipitation development and electrification in a growing convective cloud. *Atmos. Res.,* **33,** 1–24.
Willoughby, H. E., J. A. Clos, and M. G. Shoreibah, 1982: Concentric eyewalls, secondary wind maxima, and the evolution of the hurricane vortex. *J. Atmos. Sci.,* **39,** 395–411.
Winn, W. P., C. B. Moore, and C. R. Holmes, 1981: Electric field structure in an active part of a small, isolated thundercloud. *J. Geophys. Res.,* **86,** 1187–1193.
Zipser, E. J., and K. Lutz, 1994: The vertical profile of radar reflectivity of convective cells: A strong indicator of storm intensity and lightning probability? *Mon. Wea. Rev.,* **122,** 1751–1759.